Solubility of Polar and Non-Polar Aromatic Molecules in Subcritical Water: The Role of the Dielectric Constant

Nuno Galamba[a,*], Alexandre Paiva[b], Susana Barreiros[b], Pedro Simões[b]

[a] *Centre of Chemistry and Biochemistry and Biosystems and Integrative Sciences Institute, Faculty of Sciences of the University of Lisbon, C8, Campo Grande, 1749-016 Lisbon, Portugal.*

[b] *LAQV-REQUIMTE, Departamento de Química, Faculdade de Ciências e Tecnologia, Universidade Nova de Lisboa, 2829-516 Caparica, Portugal*

[*] Corresponding author. Electronic mail: njgalamba@fc.ul.pt

Abstract

Liquid water at temperatures above the boiling point and high pressures, also known as pressurized hot water, or subcritical water (SBCW), is an effective solvent for both polar and non-polar organic solutes. This is often associated to the decrease of water's dielectric constant at high temperatures, apparently allowing water to behave like an organic solvent. The decrease of the solubility at high pressures, in turn, is explained by a mild increase of the dielectric constant of water. Nevertheless, the relationship between the dielectric constant of water, hydration, and the solubility of polar and non-polar molecules in SBCW, remains poorly understood. Here, we study through molecular dynamics, the hydration thermodynamic parameters and the solubility of non-polar and polar aromatic model systems, for which a solubility increase in SBCW is observed. We show that the temperature dependence of the hydration free energy of the model non-polar solutes is non-monotonic, exhibiting a solute size independent maximum at ~475 K, above which hydration becomes entropically favorable and enthalpically unfavorable. The monotonic increase of the solubility, separated here in hydration and vaporization or sublimation components of the pure liquid or solid solute, respectively, is, in turn, related to the temperature increase of the latter, and only to a minor extent with the decrease of the hydration free energy above ~475 K, via the hydration entropy. A solubility increase or decrease is also found at high pressures for different solutes, explained by the relative magnitude of the hydration and the vaporization or sublimation components of the solubility. For the model solid polar system studied, the hydration free energy increases monotonically with the temperature, instead, and the solubility increase is caused by the decrease of the sublimation component of the solubility. Thus, despite of the observed increase of the hydration free energy with pressure, related to the entropic component decrease, our results indicate that the dielectric constant plays no significant role on the solubility increase of non-polar and polar solutes in SBCW, opposite to the dielectric constant picture. The structure of water next to the solutes is also investigated and a structural enhancement at room temperature is observed, resulting in significantly stronger pair interactions between a water molecule and its third and fourth nearest water neighbors. This structural and energetic enhancement nearly vanishes, however, at high temperatures, contributing to a positive hydration entropy.

I. Introduction

Water above the boiling point and at pressures sufficiently high (i.e., above saturation pressure) to keep water in the liquid state, aka, pressurized hot water or subcritical water (SBCW), is an effective solvent in extraction processes because of its dissolving power of both polar and non-polar organic compounds.[1–5] This constitutes a promising green selective extraction method for non-polar and polar substances, through the variation of the temperature and pressure, avoiding the use of toxic organic solvents, and therefore, especially relevant to the pharmaceutical industry[3,6].

The dissolving power of SBCW has long been related to the decrease of the dielectric constant of water with the temperature, approaching the dielectric constant of common organic solvents[1–5,7,8]. For instance, at 298 K and 1 atm, the dielectric constant of water[9] is 78.46; at 100 atm this value is 78.85, whereas at 498 K and 100 atm, the dielectric constant decreases to 31.13, already lower, for instance, than the dielectric constant of methanol (33.1)[10] at 298 K and 1 atm (see Fig. 1 of ref. [3] for a mapping of the temperature dependence of the dielectric constant of water to that of different solvents).

This picture, hereinafter referred to as the dielectric constant picture (DCP), foresees that as the temperature is increased the polarity of water molecules decreases, enhancing the solubility of non-polar solutes and reducing that of polar molecules[3]. This statement reflects the well-known "like dissolves like". The decrease of the solubility of many non-polar molecules at high pressures is also apparently consistent with this picture, since the dielectric constant of water increases with pressure.[2] The solubility of many organic molecules bearing polar groups is also observed to increase in SBCW and has also been rationalized, either by the decrease of the dielectric constant or, similarly, by a more broken hydrogen-bond (HB) network[2,3,11,12]. However, the temperature dependence of the solubility of various solutes has been shown to be significantly larger than the temperature dependence of the dielectric constant of water[13] and some solutes (e.g. benzene, 1,8-cineole) exhibit a solubility minimum, opposing this picture.[11,3] In addition, the solubility of some aromatic solutes increases at low pressures and decreases at large pressures[14], whereas the dielectric constant increases monotonically with the pressure. These observations cast doubts on the role of the dielectric constant on the solubility of non-polar and polar organic solutes. Furthermore, the relationship between the dielectric constant, the hydration thermodynamics, and the temperature and pressure dependence of the solubility remains elusive. Understanding this relationship is key to the development of accurate models[15–17] allowing predicting the solubility of different solutes at room temperature and in SBCW.[3,4]

The hydration enthalpy of any solute is in general negative, favoring solubility, whereas the entropy is negative, exerting the opposite effect. The first is governed by solute-solvent attractive interactions with a contribution from the reorganization of water's HB network upon solute

insertion, while the latter is related to the reversible work of formation of a cavity for inserting the solute, with a contribution from the reorganization of water's HB network.

For non-polar gases such as rare gases and various gaseous aliphatic hydrocarbons at room temperature, extensively studied experimentally[18–21] and through theoretical and simulation methods[22–29], the hydration free energy is positive at room temperature because the magnitude of the entropic term exceeds that of the hydration enthalpy, dominated by solute-solvent attractive dispersion interactions. The solvent excluded volume, connected to the formation of the solute's cavity, results in a reorganization of water's HB network. The nature of the former has been debated, with some studies indicating a tetrahedrality enhancement of some water molecules in the first coordination sphere of hydrophobic solutes and groups[30–36], and others reporting opposite observations[37–40]. The enthalpy and entropy contributions associated with the reorganization of water's HB network to the hydration free energy have been shown to nearly compensate, thus not influencing the hydration free energy and, therefore, the solubility[41–47]. The solubility of non-polar gases decreases at high temperatures, reaching a minimum below the boiling point of water, and monotonically increasing up to the critical temperature.[19,26]

Non-polar aromatic solutes such as benzene, liquid at room temperature, are slightly more soluble than aliphatic hydrocarbons, with a negative hydration free energy at room temperature[21,48–51]. The origin of this enhanced solubility has been debated, being either associated to benzene's ability to accept water HBs[21,49] or to benzene-water van der Waals interactions[48,51]. The solubility of benzene has a minimum around 290 K and 1 atm, increasing at high temperatures[52], whereas the hydration free energy increases, becoming positive at temperatures around the boiling temperature of water[21,48]. The solubility of other simple non-polar aromatic substances such as naphthalene or anthracene exhibit a significant increase of the solubility in SBCW, explained by the decrease of water's dielectric constant[13,53,2,3]. A large solubility increase is also observed for many other non-polar as well as polar solutes[3–5].

Here, we study through molecular dynamics simulations and "alchemical" free energy calculations, the hydration thermodynamic parameters and solubility of benzene, naphthalene, anthracene, and gallic acid, in SBCW, aiming at understanding the effect of temperature and pressure on the hydration free energy, enthalpy, and entropy, as well as on the solubility of these model substances. Further, the structure and energetics of water next to the non-polar solutes is investigated.

The remaining of the article is organized as follows: In Section II the methods used in this study are detailed, including the approach used to calculate the solubility, the hydration thermodynamic parameters, the dielectric constant of water, and the structure of water. The results for the hydration thermodynamic parameters and the solubility of the various model solutes are

discussed in Section III, along with the analysis of the structure of water in the coordination spheres of the solutes. In Section IV some conclusions are provided.

II. Methods

A. Solubility of Liquid and Solid Solutes in Water

Various approaches have been followed to compute the solubility of inorganic salts and organic molecules through molecular simulations (see [54–64] and references therein). Here, the solubility was calculated through an approach similar to that proposed by Thompson *et al.*[54], and Ahmed and Sandler[55], where the solubility of a liquid or solid solute *A* in water is calculated from its standard-state[65] hydration free energy and the standard-state solvation free energy of *A* in *A* (i.e., the solute self-solvation free energy). The hydration free energy of a solute *A*, either solid or liquid, can be related to the solubility, *s*, by[54],

$$\Delta G_{\text{hyd}} = RT \ln\left(\frac{P_A^{\bullet}}{P^{\circ}}\right) - RT \ln s \tag{1}$$

where, $P_A^{\bullet}$ is the equilibrium vapor pressure of *A* over pure *A*, P° is the pressure of an ideal gas at 1 M, at the temperature of interest, and *s* is the aqueous solubility of *A* in molarity units. Thus, the solubility can be calculated from,

$$s = \left(\frac{P_A^{\bullet}}{P^{\circ}}\right) e^{-\Delta G_{\text{hyd}}/RT} \tag{2}$$

Equations (1) and (2) assume the aqueous solution of *A* obeys Henry's law, and, therefore, that the saturated solution is infinitely dilute. In spite of this approximation, eq. (2) has been shown to hold for various liquid and solid solutes.[54,55,66,67] From eq. (2), solubility can be calculated from the hydration free energy and the pure solute *A* vapor pressure, which in turn can be obtained from the solute self-solvation free energy[54,68]. For liquid solutes the self-solvation free energy corresponds to transferring a single molecule of solute from the pure gaseous phase into the pure liquid phase, and is given by[54,68],

$$\Delta G_{\text{self}} = RT \ln\left(\frac{P_A^{\bullet}}{P^{\circ} M_A}\right) \tag{3}$$

assuming ideal behavior in both phases and where M_A is the equilibrium molarity of pure liquid *A*, which is obtained from the liquid density of *A*. The vapor pressure can, therefore, be calculated from,

$$P_A^{\bullet} = P_A^{liq} = P^{\circ} M_A e^{\Delta G_{\text{self}}/RT} \tag{4}$$

and the aqueous solubility from eq.(2). Now, substituting eq. (4) into eq. (2),

$$
\begin{aligned}
& s(T,P) = M_A e^{\Delta G_{\text{self}}(T,P)/RT} e^{-\Delta G_{\text{hyd}}(T,P)/RT} \\
& \ln s(T,P) = \left[\ln M_A + \Delta G_{\text{self}}(T,P)/RT\right] + \left[-\Delta G_{\text{hyd}}(T,P)/RT\right] \\
& \ln s(T,P) = s_{\text{vap}} + s_{\text{hyd}}
\end{aligned}
\tag{5}
$$

where s_{vap} and s_{hyd} are vaporization and hydration related components of the solubility. Equation (5) expresses the dependence of the logarithm of the solubility on the self-solvation free energy (and M_A) and the hydration free energy. Thus, solubility is favored by a large negative ΔG_{hyd} and a small (less negative) ΔG_{self} (< 0).

For a solid solute *A* the self-solvation free energy in the supercooled liquid can be calculated instead, and the solid vapor pressure corrected through the following expression[55],

$$
P_A^{solid} = P_A^{\bullet} \exp\left(\frac{\Delta S_{fus}}{R}\left(1 - T_m / T\right) \right) \tag{6}
$$

where, ΔS_{fus} is the fusion entropy, T_{m} is the melting temperature, $P_A^{\bullet}$ is given by eq.(4), and eq.(3) corresponds now to the transfer of a single molecule of solute from the pure gaseous phase to the solid, approximated by the pure supercooled phase. Now, using,

$$
\Delta G_{\text{self}}^{solid} = RT \ln\left(\frac{P_A^{solid}}{P^{\circ} M_A} \right) \tag{7}
$$

the solubility can be written as,

$$
\begin{aligned}
& s(T,P) = M_A e^{\Delta G_{\text{self}}(T,P)/RT} e^{-\Delta G_{\text{hyd}}(T,P)/RT} \\
& \ln s(T,P) = \left[\ln M_A + \Delta G_{\text{self}}(T,P)/RT\right] + \left[-\Delta G_{\text{hyd}}(T,P)/RT\right] \\
& \ln s(T,P) = s_{\text{sub}} + s_{\text{hyd}}
\end{aligned}
\tag{8}
$$

where M_{A} is the molarity of solid *A*, approximated by the molarity of the supercooled pure liquid, and s_{sub} and s_{hyd} are sublimation and hydration related components of the solubility. Eq. (6) was used for the solid solutes with the following experimental values of ΔS_{fus}: Naphthalene ΔS_{fus} = 53.21 J/molK[69], Anthracene ΔS_{fus} = 59.2 J/molK[69], and gallic acid, $\Delta S_{fus} = \Delta H_{fus} / T_m$ = 119 J/molK[70,71]; gallic acid appears to decompose upon melting[72] and this value may, therefore, be subject to some uncertainty.

We note that, although the self-solvation free energy in the solid, rather than in the supercooled liquid, may be computed[59,64], avoiding eq. (6), this requires knowledge of the crystal structure of the solutes at the thermodynamic states of interest. The latter, in turn, often includes different polymorphs, not always identified. We believe, however, the difference between these approaches should be small, relative to the inaccuracy associated with the use of the same force field for studying hydration and the pure solute supercooled liquid or solid phase. For the purpose

of this study, we will see that the latter should not influence our conclusions.

The solubility, *s*, in eq. (2) in molarity units can be converted to mol fraction, x_S, often used to express solubility, by the following relation, $x_S = s/\left(s + 1000/M_w\right)$, for a density of water equal to 1 g·cm^{-3} and where M_w is the molecular weight of water. The temperature and pressure variation of the density of water has a small effect on the solubility and therefore the last equation can be used to a good approximation.

B. Simulation Details

Molecular dynamics (MD) simulations of the following non-polar and polar solutes in water were performed with the Generalized AMBER Force Field (GAFF)[73] and the TIP4P-Ew[74] water model: benzene (T_m = 279 K; T_b = 353 K)[69], naphthalene (T_m = 353 K; T_b = 490 K)[69], anthracene (T_m = 490 K; T_b = 613 K)[69], and gallic acid (T_m = 524.2 K)[70,71], where T_m and T_b are respectively the normal melting and boiling temperatures. A larger melting temperature for gallic acid, T_m = 535 K[72], was also reported. Furthermore, since decomposition is observed upon melting[72], as previously noted, gallic acid has no T_b. Thus, with exception of benzene the solutes studied are solid at room temperature and pressure. The polar system chosen was gallic acid because its solubility has been assessed experimentally, depicting an exponential increase in SBCW[12,75,76] similar to that observed for many non-polar aromatic molecules. The dipole moment of gallic acid in the gas phase was estimated here at the MP2[77]/cc-pvdz[78] theoretical level and found to be 2.75 D. The experimental dipole moment of gallic acid could not be found in the literature.

The force field was derived following the GAFF approach. The geometry optimizations and the Merz-Kollman[79,80] charges were calculated with GAUSSIAN 09[81]. The geometries were optimized through DFT[82,83] at the B3LYP[84,85]/cc-pvdz[78] theoretical level and the atomic charges were calculated at the HF/6-31G* level with RESP[86]. Despite the TIP3P water model[87] provides in general more accurate ΔG_{hyd} values, we chose the TIP4P-Ew model because it provides a more accurate description of liquid water. The GAFF force field with TIP4P-Ew, in turn, resulted in a more accurate ΔG_{hyd} for benzene at 298 K and 1 atm, than the OPLS-aa[88], thus, defining our choice of the force field.

The MD were performed with GROMACS 5.1.4[89]. Typical SBCW extraction processes are performed at pressures between 1 atm and 100 atm. Thus, the hydration free energy of the solutes was calculated at temperatures ranging between 298 K and 598 K, at 1 atm and 100 atm. For the non-polar solutes, however, calculations were also performed at pressures ranging between 100 atm and 1000 atm – 2500 atm at a single temperature (398 K), to study the effect of pressure on the hydration thermodynamic parameters and solubility. The aqueous systems were comprised of a

single molecule of solute and 1000 water molecules in a cubic box with periodic boundary conditions. The dielectric constant (see Section II-D) was also calculated for pure TIP4P-Ew water at similar temperatures and pressures for a system comprised by 500 water molecules. The simulations of the pure solutes to calculate the self-solvation free energy were performed for 256 molecules. For the pure water dielectric constant and the free energy calculations, the systems were first equilibrated for 100 ps in the *NVT* ensemble followed by 5 ns in the *NpT* ensemble. The dielectric constant was then calculated through block averaging over four independent simulations of 10 ns in the *NpT* ensemble.

The equations of motion for the simulation of pure water and the equilibration of the aqueous solutions and the pure solutes were solved with the Verlet leap-frog algorithm with a 2 fs time-step for water and the aqueous solutions, and 1 fs for the pure solutes. The T and p were controlled with the thermostat of Bussi *et al.*[90] and the Parrinello-Rahman barostat[91]. Electrostatic interactions were computed with the particle-mesh Ewald (PME) method[92]. A cut-off of 1 nm was used for non-bonded van der Waals and for the PME real space electrostatic interactions. Heavy atom-hydrogen covalent bonds were constrained with the LINCS algorithm[93].

C. Free Energy, Entropy, and Enthalpy Calculations

While hydration free energies are generally difficult to assess experimentally, various methods have been proposed to calculate solvation free energies through molecular simulations.[94–98] Here, we performed "alchemical" free energy calculations with the Bennett acceptance ratio (BAR)[99] method, as implemented in GROMACS, to predict both the hydration free energies and the self-solvation free energies involved in the calculation of the solubility through eqs (5) and (8). Alchemical free energy calculations are based on the definition of a parameter, λ, taking values in the interval [0,1], allowing connecting the states A (λ=1) and B (λ=0) defined by the Hamiltonians $\mathbf{H}_A(r,p;\lambda)$ and $\mathbf{H}_B(r,p;\lambda)$. The transition from state A, here the solute in water or in the pure liquid or supercooled liquid, and the state B, the solvent or the pure solute, is performed by a number (N_λ) of different values of λ corresponding to non-physical states. A decoupling approach was used for $N_\lambda = 28$ connecting the states A and B. For Coulombic interactions decoupling, a $\Delta\lambda$ = 0.05 was adopted. For the van der Waals interactions decoupling, a similar $\Delta\lambda$ was used with additional points separated by $\Delta\lambda = 0.025$ at $\lambda > 0.7$. The free energy was further calculated including additional values of λ for Coulombic and dispersion interactions decoupling, for comparison purposes. The latter showed no significant differences for the various systems, indicating adequate sampling. Langevin stochastic MD[100] was carried out and a soft-core potential was used for Lennard-Jones and electrostatic interactions to avoid numerical singularities at

terminal λ values, with α = 0.5, σ = 0.3, and a soft-core power of 1.[96,101–104] The simulations for each λ consisted of a steepest descent energy minimization step, followed by a 0.5 ns Langevin *NVT* simulation, and a 1 ns Langevin simulation in the *NPT* ensemble, using the Parrinello-Rahman barostat[91]. The hydration free energy was then computed from two independent Langevin *NPT* simulations, 5 ns long, for each λ. For some temperatures, where larger differences were observed, up to 5 independent simulations, 5 ns long, were carried out.

The entropy was calculated from, $\Delta S_{\mathrm{hyd}} = -\left(\partial \Delta G_{\mathrm{hyd}} / \partial T\right)_{N,P}$, where ΔG_{hyd} was fitted to a second order polynomial, and the hydration enthalpy from, $\Delta H_{\mathrm{hyd}} = \Delta G_{\mathrm{hyd}} + T\Delta S_{\mathrm{hyd}}$. The entropy was also estimated from the numerical derivative of ΔG_{hyd}. The latter was found to be in qualitative agreement with that obtained from the quadratic polynomial derivative. For comparison purposes we also calculated the hydration enthalpy at different temperatures and pressures, through[96],

$$\Delta H_{hyd} = \Delta U_{hyd} + p\Delta V = U_{\mathrm{solution}} - (U_{\mathrm{water}} + U_{\mathrm{solute}}) + p\Delta V \qquad (9)$$

where U_{solution} is the internal energy of the aqueous solution, U_{water} is the internal energy of pure water at the same *N*, *p*, and *T*, U_{solute} is the internal energy of the solute in vacuum at the same *T*, and the last term is the *pV* work associated to the volume change in the hydration process. The calculation of ΔH_{hyd} through eq. (9) is hampered by the large fluctuations that characterize water-water interactions. Here, ΔH_{hyd}, was calculated from ten independent trajectories, 10 ns long, for the aqueous solution, pure water, and the solute in vacuum. We note that every approach to find either ΔH_{hyd} or ΔS_{hyd}, suffers from limitations[96,105] and, therefore, the latter are less accurate than ΔG_{hyd}.

D. Dielectric constant

For any rigid non-polarizable water model, such as that used in this study (TIP4P-Ew)[74] the dielectric constant cannot decrease with the temperature via the dipole moment of the water molecules, which is constant, depending, therefore, only on the structure of the liquid, characterized by a lower tetrahedrality and an increasing number of broken HBs. The dipole moment of the water molecule in the gas phase is 1.85 D. The experimental dipole moment of liquid water is 2.9 ± 0.6 D.[106] That of the TIP4P-EW molecule is 2.32 D, whereas theoretical values between 2.3-3.1 D have been proposed for the dipole moment in the condensed phase[107–120]. The increased dipole moment of water in the bulk, relative to the gas phase, is caused by polarization effects induced by neighbor

molecules and intra-molecular geometry fluctuations connected to the formation of HBs. There is no experimental data on the variation of the dipole moment with the temperature (and pressure) in the liquid phase, although this is expected to decrease because of the lower number of HBs at high temperatures. A reduction of the dipole moment of water molecules is observed, however, through computer simulations, at high temperatures[108,111] and in the liquid-vapor interface[114,116,119], relative to the bulk, consistent with this view.

The dielectric constant of water has been previously calculated for various water models[121] including the TIP4P-Ew water model[122]. The latter studies showed qualitative, and in some cases quantitative agreement with the experimental dielectric constant. We assessed the dielectric constant of TIP4P-Ew water between 298 K and 378 K at 1 atm and between 298 K and 598 K at 100 atm, and at 398 K at pressures between 100 atm and 2500 atm. The dielectric constant was calculated from the fluctuations of the dipole moment of the system[123], $\mathbf{M} = \sum_i q_i \mathbf{r}_i$, where q_i and $\mathbf{r}_i$ are, respectively, the charge and position of particle *i*, as,

$$\varepsilon = 1 + \frac{4\pi}{3k_B TV}\left(\left\langle \mathbf{M}^2 \right\rangle - \left\langle \mathbf{M} \right\rangle^2\right) \tag{10}$$

where k_B is Boltzmann's constant, *V* is the volume, and *T* is the temperature.

Figure 1 shows that the dielectric constant of TIP4P-Ew water, although lower than ε of real water, decreases monotonically with the temperature and increases monotonically with the pressure, qualitatively consistent with the behavior of real water.

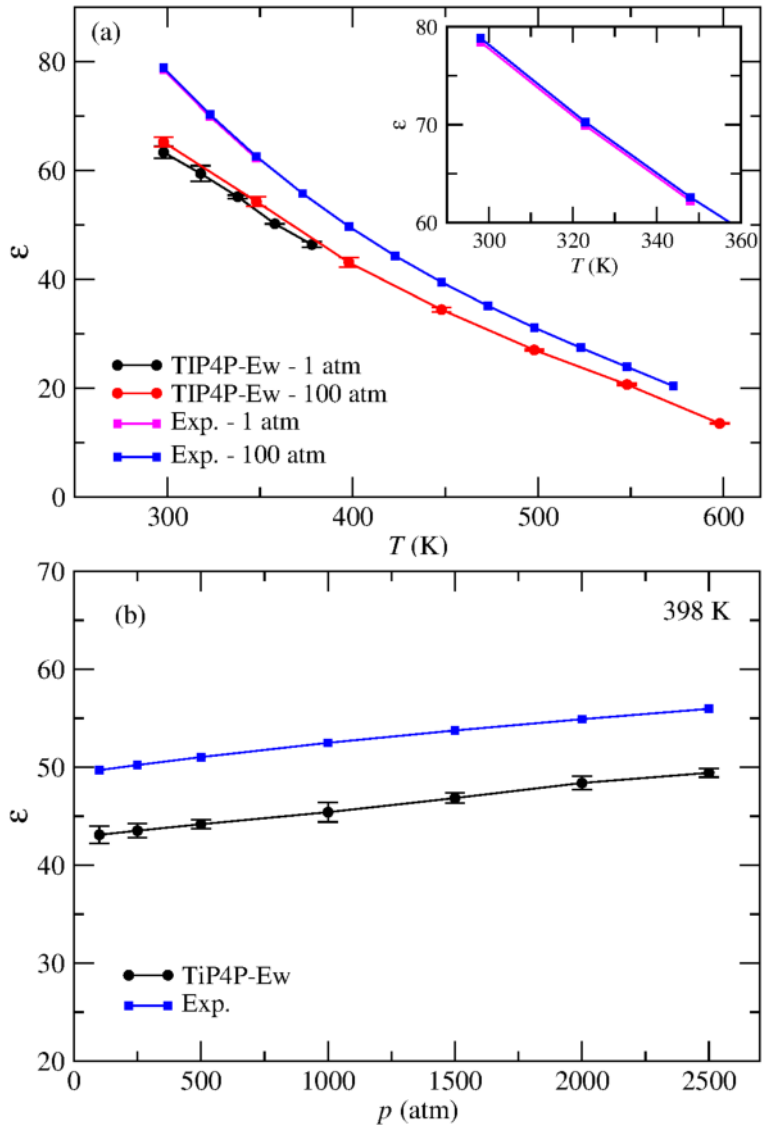

Figure 1 – (a) Temperature dependence of the dielectric constant, ε, of TIP4P-Ew water (this work) and real water[9] at 1 atm and 100 atm, showing the decrease (increase) of ε with the temperature (pressure). (b) Pressure dependence of the dielectric constant of TIP4P-Ew water (this work) and real water[9] at 398 K. Error bars are standard deviations calculated from 4 independent trajectories.

Notice that any solubility increase (decrease) associated to the decrease (increase) of the dielectric constant of water with the temperature (pressure) must occur through a decrease (increase) of the hydration free energy and, therefore, through the increase of the s_{hyd} component in eqs (5) and (8).

E. Solute-Water and Water-Water Structure

The structure of water in the bulk and in the hydration shells (HSh) of the solutes was assessed through the calculation of the solute-water radial distributions functions (rdf), the local structure index (LSI)[124], and the tetrahedrality[125,126] of water. Further, distributions, $P(O\cdots O_n)$, of

the distance from each oxygen atom to the nth (n = 1 to 5) nearest oxygen atom of neighbor water molecules and the distribution, $P(O\cdots H)$, of the distance of each oxygen atom to the nearest 2 H atoms of neighbor water molecules, were calculated. The respective pair interaction energies, $P(W\cdots W_n)$, between a water molecule and its nth (n = 1 to 5) nearest water molecule were also computed.

The LSI is defined by,

$$\mathrm{LSI} = \frac{1}{n}\sum_{i=1}^{n}\left[\Delta(i) - \bar{\Delta}\right]^2 \tag{11}$$

where $\Delta(i) = r_{i+1} - r_i$, r_i is the distance of molecule i from a central water molecule, $\bar{\Delta}$ is the $\Delta(i)$ average, $\bar{\Delta} = \frac{1}{n}\sum_{i=1}^{n}\Delta(i)$, and water molecules are ordered around a central water molecule according to their distance, that is, $r_1 < r_2 < ... < r_i < r_{i+1} < ... < r_n < 3.7\text{Å} < r_{n+1}$. Although not assessing directly the tetrahedrality of water, larger LSI values are found for more tetrahedral water because of water exclusion in the region between the first (r ~ 3.3-3.5 Å) and second HSh, whereas a value close to zero is obtained for randomly distributed water molecules.[124] The tetrahedrality was directly assessed through the calculation of the orientational order parameter[125], q, in the rescaled form[126], $q = 1 - \frac{3}{8}\sum_{i=1}^{3}\sum_{j=i+1}^{4}\left(\cos\theta_{ij} + 1/3\right)^2$, where θ_{ij} is the angle formed by the lines joining the O atom of a given water molecule and those of its nearest neighbors, i and j. The average value of q varies between 0 (ideal gas) and 1 (perfect tetrahedral HB network). This parameter requires that a water molecule has four nearest water neighbors. Thus, analysis of q may be misleading when water molecules closer to the solute than to the four nearest water neighbors are probed. These molecules cannot form up to four HBs and are not, therefore, tetrahedral.[31] This is illustrated in Fig. 1-SI, which shows the distribution of the distance from each O atom to the fourth nearest O atom, $P(O\cdots O_4)$, in the bulk and in the first and second HSh of the carbon atoms of benzene. The water molecules with four or more water neighbors (4MWN) show a contraction of the $O\cdots O_4$ distance whereas those with less than four water neighbors (L4WN) exhibit a long distance tail, relative to bulk water. The second closest H atom of a neighbor molecule is also shifted to larger distances, relative to bulk water, and opposite to water molecules with 4MWN (see Fig. 1-SI). Thus, we restrict the tetrahedrality analysis to water molecules with 4MWN in the first and second HSh of the carbon atoms of the solutes. However, energetic analysis, $P(W\cdots W_n)$, is performed for water molecules with 4MWN and L4WN.

III. Results and Discussion

A. Hydration Free Energy, Enthalpy, and Entropy

Figure 2 depicts the hydration free energy, entropy, and enthalpy of benzene aqueous solutions at 1 atm and 100 atm. ΔG_{hyd} increases with the temperature at 1 atm (Fig. 2a) up to the boiling temperature of water (the highest temperature simulated is actually already 5 K above the experimental T_b), consistent with experimental data. The negative ΔG_{hyd} at low temperatures is associated to the larger magnitude of ΔH_{hyd}, relative to $T\Delta S_{hyd}$. However, above ~330 K an opposite trend is observed and ΔG_{hyd} becomes positive. Figure 2b shows that at 100 atm ΔG_{hyd} increases at low temperatures, similar to ΔG_{hyd} at 1 atm, because, despite of the increase of $T\Delta S_{hyd}$, the hydration enthalpy increases at a faster rate, opposing hydration. However, at ~ 475 K, ΔG_{hyd} shows a maximum associated to a larger rate of increase of $T\Delta S_{hyd}$, relative to ΔH_{hyd}, at high temperatures.

The $T\Delta S_{hyd}$ increase with the temperature at 1 atm and 100 atm suggests a facilitated insertion of the solute in water, explained by the increasing number of broken HBs, enhancing the average distance between water molecules, and, thus, the size of voids in the liquid. The average nearest neighbor distance, $r_{O\cdots O_1}$, provides a simple probe of the size of voids in the liquid, approximated by the spherical shell of volume, $V_{void} = (4/3)\pi(r_{O\cdots O_1})^3 - V_{H_2O}$, where V_{H_2O} is the volume of a molecule of water approximated by a sphere. Figure 2-SI shows a shift of the $P(O\cdots O_1)$ distribution to larger distances and the appearance of a long tail at high temperatures, indicating the existence of larger voids in liquid water. Thus, the average distance increases from 2.7 Å to 2.8 Å (ΔV_{void} ~10 Å^3), from 298 K to 598 K, whereas the distribution upper-tail "limit" increases from ~3.2 Å to ~4.5 Å (ΔV_{void} ~240 Å^3).

The ΔH_{hyd} increase with the temperature, in turn, can be explained by the less favorable solute-water interactions, $U_{sol\text{-}wat}$, (Fig. 3-SI), concomitant with the water depletion near benzene (Fig. 4-SI). The benzene-oxygen rdfs, depicted in Fig. 4-SI, show the collapse of the coordination spheres at high temperatures. Figure 3-SI also shows that solute-water van der Waals interactions are significantly more important than Coulombic interactions. The latter are related to the formation of ~1.5 HBs between benzene and water, nearly absent at high temperatures (Fig. 4-SI).

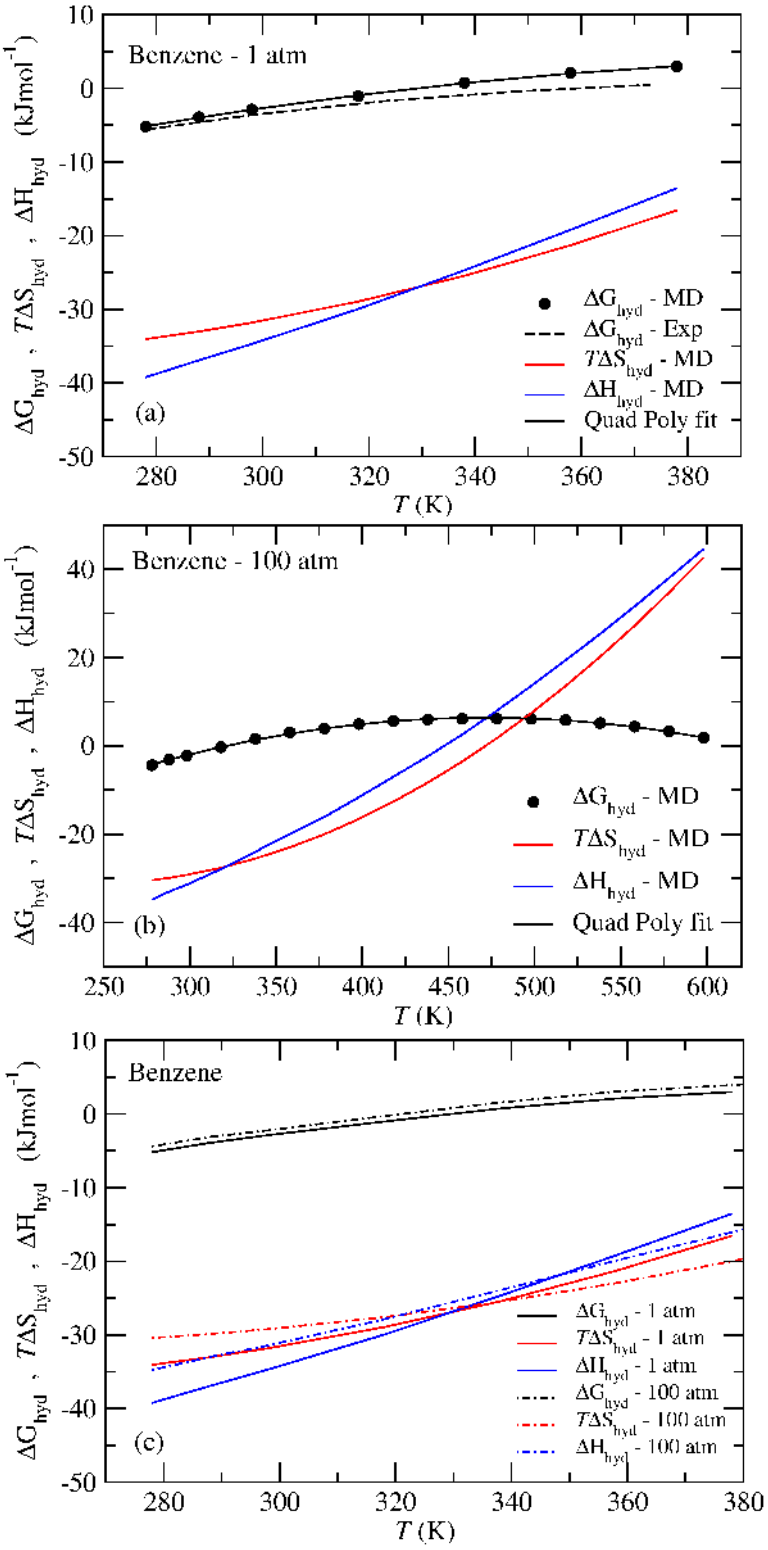

Figure 2 – Temperature dependence of the hydration free energy, ΔG_{hyd}, entropy, $T\Delta S_{hyd}$, and enthalpy, ΔH_{hyd}, in TIP4P-Ew water for benzene at (a) 1 atm and (b) 100 atm. Experimental hydration free energies[21,48] are shown. The solid black curves are fits to a quadratic polynomial used to calculate ΔS_{hyd}. (c) Comparison between ΔG_{hyd}, $T\Delta S_{hyd}$, and ΔH_{hyd} at 1 atm and 100 atm. Free energy standard deviations from block averages are lower than 0.3 kJmol^{-1} for every temperature and lower than 0.1 kJmol^{-1} for most temperatures.

We note that $U_{sol\text{-}wat}$ in Fig. 3-SI is the short-range component of the potential energy, since

the PME reciprocal space component of the electrostatic potential energy cannot be separated into solute-water and water-water components. However, calculation of $U_{\text{sol-wat}}$ using a spherical cut-off, $r_c = L/2$, where L is the length side of the MD box, without PME, gives qualitatively similar results.

Further, an increase of $T\Delta S_{\text{hyd}}$ and ΔH_{hyd} with the temperature, related to the reorganization of water's HB network is expected, because of water depletion near the solute. Despite these should nearly compensate, not significantly affecting the hydration free energy, they contribute to $T\Delta S_{\text{hyd}}$ and ΔH_{hyd}. The structure of water and its possible effect on the hydration entropy and enthalpy shall be discussed in Section III-C.

Figure 2(c) compares the hydration thermodynamic parameters for aqueous benzene at 1 atm and 100 atm. ΔG_{hyd} increases slightly with pressure and a lower (more negative) ΔH_{hyd} and $T\Delta S_{\text{hyd}}$ are observed at 1 atm, relative to 100 atm, at room temperature; $\Delta\Delta H_{\text{hyd}} = \Delta H_{\text{hyd}}(298\text{ K},1\text{ atm}) - \Delta H_{\text{hyd}}(298\text{ K},100\text{ atm})$ is ~ -3.0 kJmol^{-1}. Larger ΔH_{hyd}, by ~10 kJmol^{-1}, were found through eq. (9) (see Table 1-SI). Furthermore, large fluctuations, related to water-water interactions, hamper the precision of $\Delta\Delta H_{\text{hyd}}$. The difference between the solute-water potential energy at 1 atm, $U_{\text{sol-wat}}$ = -60.3±0.1 kJmol^{-1}, and 100 atm, $U_{\text{sol-wat}}$ = -60.4±0.1 kJmol^{-1}, in turn, is almost negligible and cannot account for the $\Delta\Delta H_{\text{hyd}}$ difference, suggesting the latter should be related instead with water-water interactions and with the $\Delta(p\Delta V)$ term, which was found to be ~ -0.84±0.04 kJmol^{-1}.

The negative entropic difference, $\Delta\Delta S_{\text{hyd}} = \Delta S_{\text{hyd}}(298\text{ K},1\text{ atm}) - \Delta S_{\text{hyd}}(298\text{ K},100\text{ atm})$, in turn, cannot be accounted by the increase of the size of voids in the liquid, since a density increase is observed, without a re-organization of the HB network resulting in larger voids in the liquid. Hence, ρ = 0.995±0.0001 g·cm^{-3} at 1 atm and ρ = 0.999±0.0001 g·cm^{-3} at 100 atm whereas $r_{\text{O}\cdots\text{O}_1}$ is nearly identical (~2.700 Å). In addition, although $T\Delta S_{\text{hyd}}$ and ΔH_{hyd} increase with the temperature at both pressures, a crossover of $T\Delta S_{\text{hyd}}$ at ~330 K and of ΔH_{hyd} at ~345 K, between the 1 atm and 100 atm curves, is observed. Thus, at high temperatures, $T\Delta S_{\text{hyd}}$ becomes less favorable and ΔH_{hyd} becomes more favorable at 100 atm than at 1 atm, and $\Delta\Delta H_{\text{hyd}} = \Delta H_{\text{hyd}}(378\text{ K},1\text{ atm}) - \Delta H_{\text{hyd}}(378\text{ K},100\text{ atm})$ is, therefore, positive, ~ +2.5 kJmol^{-1}. This change of sign, in passing from 298 K to 378 K, could not be definitely established through eq. (9), because of large fluctuations, as previously discussed (see Table 1-SI). A negligible difference between the solute-water interactions at 1 atm, $U_{\text{sol-wat}}$ = -51.7±0.1 kJmol^{-1}, and 100 atm, $U_{\text{sol-wat}}$ = -51.9±0.1 kJmol^{-1}, as well as between the average nearest neighbor distance (~2.720 Å), is also found at 378 K. Thus, the change of sign of $\Delta\Delta H_{\text{hyd}}$ should be mainly related to water-water

interactions. We stress, however, that the ΔH_{hyd} and $T\Delta S_{hyd}$, displayed in Fig. 2, are less accurate than the ΔG_{hyd}, depending on the temperature range and the number of ΔG_{hyd} values used to fit the quadratic polynomial.

We now extend the discussion to the naphthalene and anthracene aqueous solutions at 1 atm and 100 atm (see Fig. 3). ΔG_{hyd} decreases with the solute size, showing a solute size independent maximum at ~475 K. This contrasts with previous simulation results that predicted a positive hydration free energy difference between naphthalene and benzene and between anthracene and naphthalene at 300 K and 1 atm.[50] Despite ΔG_{hyd} of the solutes was not calculated in that study, only the difference, the reason behind this inconsistency is not clear. Here, we found the following values for ΔG_{hyd} at 298 K and 1 atm: ΔG_{hyd} = -2.9 kJmol^{-1}, ΔG_{hyd} = -5.6 kJmol^{-1}, and ΔG_{hyd} = -9.6 kJmol^{-1}, for benzene, naphthalene, and anthracene, respectively. Although larger (less negative), these are in qualitative agreement with experimental data: ΔG_{hyd} = -3.6 kJmol^{-1} (ref.[21]) and ΔG_{hyd} = -5.4 kJmol^{-1} (ref.[127]) for benzene; ΔG_{hyd} = -9.6 kJmol^{-1} for naphthalene[128]; and ΔG_{hyd} = -17.7 kJmol^{-1} for anthracene [128]. Our results are also consistent with those previously obtained through MD for the OPLS-aa force fields and distinct water models[64,128].

The free energy maximum at ~475 K corresponds to a zero $T\Delta S_{hyd}$ ($\Delta S_{hyd} = -\left(\partial \Delta G_{hyd} / \partial T\right)_{N,P} = 0$; see Fig. 3b), suggesting the existence of large voids in water at $T \geq$ ~475 K, and thus, the reversible work of formation of a cavity for solute insertion is zero for the solute sizes studied. Hence, above 475 K the entropy should be governed instead by the reorganization of the HB network of water around the solute. This is further discussed in Section III-C.

The decrease of ΔG_{hyd} with the solute size at low temperatures is associated to a lower ΔH_{hyd}, whereas at high temperatures this is related, instead, to a larger $T\Delta S_{hyd}$. Figure 3-SI shows that although $U_{sol\text{-}wat}$ decreases with the solute size at every temperature, the rate of increase of $U_{sol\text{-}wat}$ at high temperatures increases with the solute size, reducing the differences between the solutes. Further, van der Waals interactions exhibit a larger decrease with the solute size, than Coulombic interactions, and the reduction of the $U_{sol\text{-}wat}$ differences at high temperatures is caused by a lower difference between the former, showing that $U_{sol\text{-}wat}$ is governed by van der Waals interactions. Nonetheless, this indicates that water-water interactions, and thus the HB reorganization around the solutes, play a significant and differential role, for different size solutes.

The increase of $T\Delta S_{hyd}$ with the solute size above ~475 K is particularly interesting, suggesting that insertion of a large solute in water is entropically facilitated, over a small solute, at high enough temperatures. We surmise this is related with the HB reorganization around the distinct

solutes at high temperatures, supporting the idea that at high enough temperatures (> ~475 K) $T\Delta S_{hyd}$ is governed by the latter contribution to the entropy as above mentioned (see Section III-C).

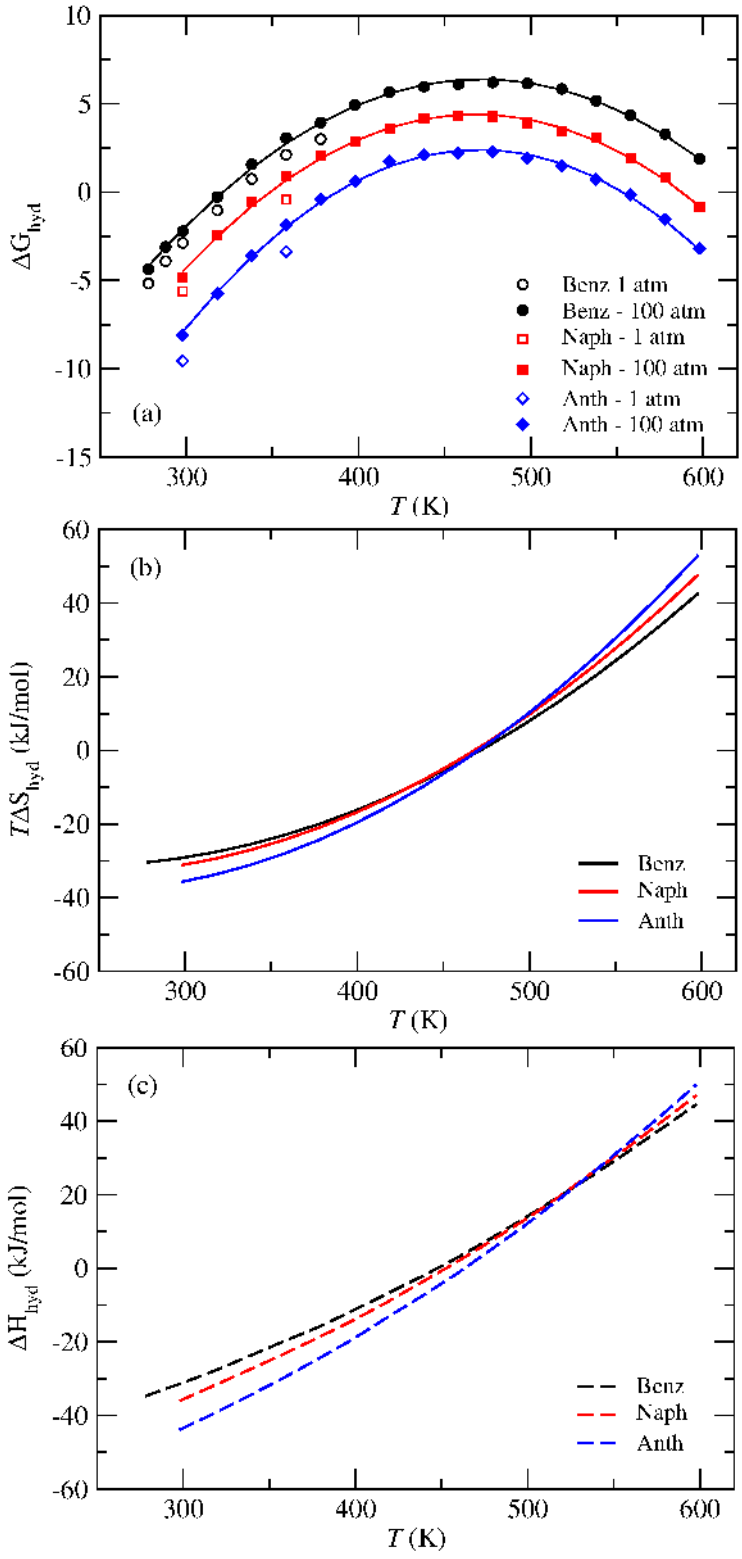

Figure 3 – (a) Hydration free energy, (b) entropy ($T\Delta S_{hyd}$), and (c) enthalpy, at 100 atm for benzene, naphthalene, and anthracene. The free energies calculated at 1 atm at various temperatures are also shown. The solid curves in (a) at 100 atm are fits to quadratic polynomials used to calculate the hydration entropy shown in (b). Free energy standard deviations from block averages are lower than 0.3 kJmol^{-1} for every temperature and lower than 0.1 kJmol^{-1} for most temperatures.

We consider now the case of the polar system, gallic acid in water. Figure 4 shows that ΔG_{hyd} of gallic acid increases with the temperature, both at 1 atm and 100 atm**,** in contrast with the non-polar solutes, and apparently consistent with the DCP, in that lower dielectric constant water is a poor solvent for polar solutes. Thus, the solubility increase of gallic acid[12,75,76] with the temperature cannot be related neither to the dielectric constant decrease nor with a more broken HB network of water, as previously suggested[12], but rather with the increase of the sublimation component of the solubility, related to the vapor pressure of the solid (see Section II-B).

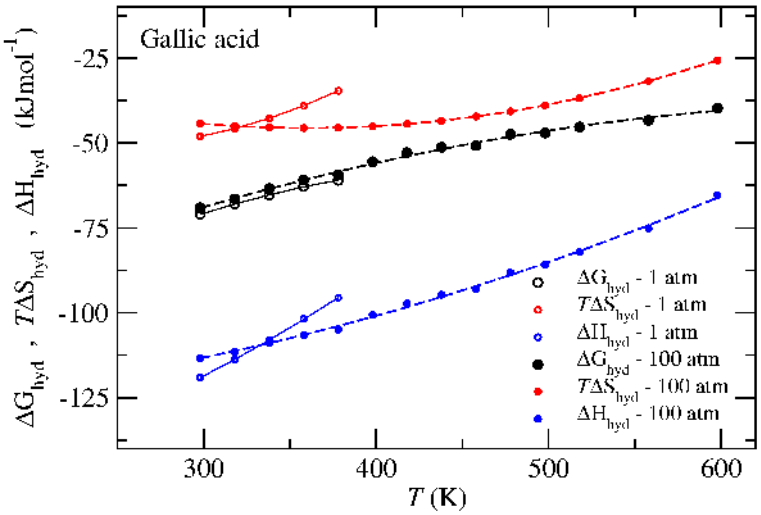

Figure 4 – Temperature dependence of the hydration thermodynamic parameters for gallic acid at 1atm and 100 atm. Lines are fits to quadratic polynomials.

B. Solubility

Figure 5 shows the solubility of benzene, naphthalene, and anthracene in water at 1 atm and 100 atm along with the hydration, s_{hyd}, and the vaporization, s_{vap}, and sublimation, s_{sub}, components. The ΔG_{self} for pure benzene, naphthalene, and anthracene at 1 atm and 100 atm are displayed in Fig. 6(a)-SI. We recall that the decrease of the dielectric constant of water can only influence the solubility through the hydration component, whereas s_{vap} and s_{sub} depend on the vapor pressure of the pure solutes (see eqs (4) and (6)). A solubility minimum can be observed for benzene, although shifted to a larger temperature (~338 K), relative to the experimental minimum at ~290 K[52,129]. Furthermore, the general agreement with the experimental solubility is only qualitative, indicating that the force field and the approximations involved in the solubility calculation have limitations. For naphthalene and anthracene, a better agreement is found. We note that the solubility measurements were performed at variable pressure[2,130], in contrast with our results. The former, however, are relatively low and have a minor effect on the solubility, as further demonstrated here.

The solubility increase with the temperature, below ~475 K, is caused by the s_{vap} and s_{sub}

components, whereas s_{hyd} decreases with the temperature, disfavoring the solubility. For T > 475 K the entropy increase (see Fig. 3) causes a decrease of ΔG_{hyd}, enhancing the s_{hyd} component of the solubility. The latter, however, is lower than the vaporization and the sublimation (except for anthracene) components and the solubility increase is still governed by s_{vap} and s_{sub}. Hence, at temperatures below ~475 K the solubility increase is not related to the hydration free energy, and, therefore, to the decrease of the dielectric constant. For temperatures above ~475 K, hydration has a minor positive effect on the solubility, via $T\Delta S_{hyd}$. These results contrast, with the DCP, which connects the solubility increase in subcritical water to the decrease of the dielectric constant of water with the temperature. Thus, the DCP foresees an enhancement of the solute-water interactions, related to a lower dielectric constant, and therefore a solubility increase via ΔH_{hyd}, similar to polar, relative to non-polar solutes, in water at room temperature. Furthermore, despite the TIP4P-Ew water model is rigid and non-polarizable it predicts the correct rate of decrease of the dielectric constant with the temperature (see Fig. 1), indicating that geometry fluctuations and polarization effects should not change this picture.

Figure 5 also shows that the solubility of the solutes slightly increases at 100 atm, relative to the solubility at 1 atm. This is consistent with experimental solubility data of various non-polar aromatic systems at moderate pressures, where a solubility maximum is observed[14], and contrasts with the minor increase of the dielectric constant of water (see Fig. 1). This solubility increase is caused by the s_{vap} and s_{sub} components, whereas s_{hyd} has the opposite effect. Thus, although the minor increase of ΔG_{hyd} and the decrease of s_{hyd} with pressure could be related to the increase of the dielectric constant (see discussion below), consistent with the DCP, a minor net increase of the solubility, related to the s_{vap} and s_{sub} components, is observed.

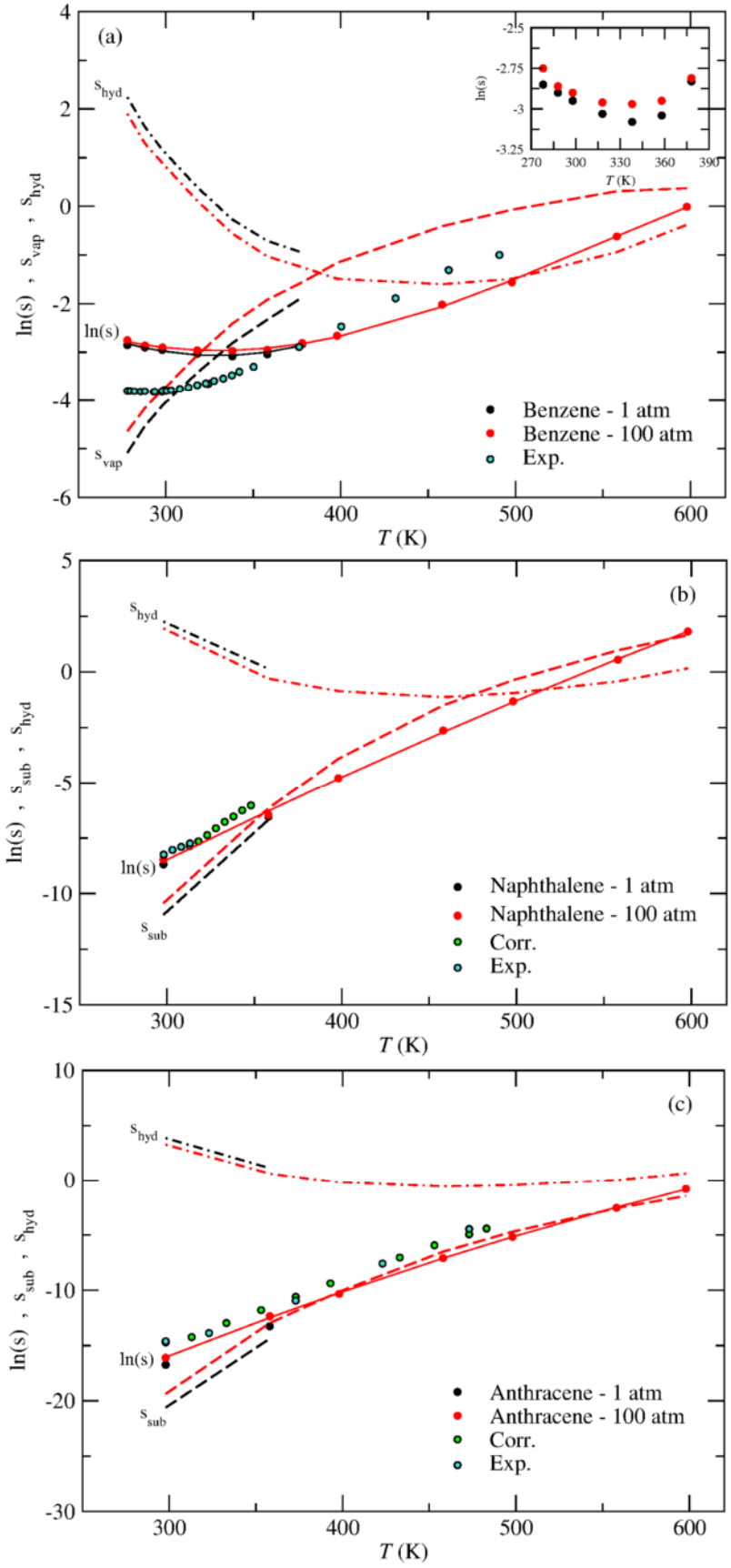

Figure 5 – Temperature dependence of the solubility of benzene, naphthalene, and anthracene at 1 atm and 100 atm. The molecular dynamics results are compared to the experimental solubility of benzene[129,130], naphthalene[131], and anthracene[2]. The solubility of naphthalene and anthracene from the semi-empirical correlation of ref.[132] given in Table 2 of ref.[3] are also shown.

To further investigate the pressure dependence of the solubility we calculated the solubility of benzene, naphthalene, and anthracene at 398 K at various pressures (see Fig. 6). The pressure dependence of ΔG_{hyd} and ΔG_{self} is shown in Fig. 7-SI. Interestingly, the solubility of benzene increases up to the highest pressure studied (2500 atm), consistent with experimental data[133], whereas that of naphthalene and anthracene display a maximum at relatively low pressures (~250 atm), similar to the solubility of other aromatic systems (alkylbenzenes)[14]. For naphthalene and anthracene at 298 K no solubility maximum is observed from experiments.[134,135] However, the solubility between 1 atm and ~440-490 atm is not reported in those studies, and the solubility, relative to that at 298 K and 1 atm, exhibits a monotonic decrease up to pressures around 2000 atm. A decrease of the solubility of OPLS-aa naphthalene in SPC[136] water with pressure, at 298 K, was also recently reported by Li *et al.*[64]. However, no solubility is reported between 1 atm and ~500 atm. Here, in spite of a weak pressure dependence of the solubility a maximum is observed at low pressures for naphthalene and anthracene. Nonetheless, the possibility that this maximum could be an artifact of the force field or of the approximations involved in the calculations of the solubility cannot be ruled out.

From Fig. 6, benzene seems to be an exception, with respect to the pressure dependence of the solubility. Nonetheless, the hydration component disfavors the solubility, for benzene, naphthalene, and anthracene, consistent with the DCP. Furthermore, the pressure dependence of the solubility is relatively small, in accordance with the mild increase of the dielectric constant of water with pressure. However, for benzene, s_{vap} increases at a faster rate than s_{sub} for the larger (solid) solutes, relative to the hydration component, explaining the solubility increase. For naphthalene and anthracene, the maximum at 250 atm results from a higher rate of increase of the sublimation component, s_{sub}, at low pressures. Thus, a decrease of the rate of increase of the sublimation component can be observed above 250 atm that causes the solubility to be governed by the hydration component, opposite to benzene. These results suggest, therefore, that opposite to the increase of the solubility at high temperatures and low pressures, the pressure dependence of the solubility of naphthalene and anthracene, could be, to some extent, related to the increase of the dielectric constant of water.

The increase of ε with pressure can be rationalized through the volume reduction and the enhanced interaction between water molecules. Thus, although the water-water pair interaction energy between the nth (n = 1 to 4) first neighbors increases (less negative) with pressure, those between more distant neighbors (n > 4) decrease, resulting in a lower water-water potential energy (see Section III-C). We note that in spite of a lower tetrahedrality, weakening HBs, pressure does not cause a decrease of the number of geometric HBs in liquid water.[137] A similar effect is observed

for the solute-water interactions (see Fig. 3-SI(b)), suggesting a decrease (more negative) of ΔH_{hyd} with pressure.

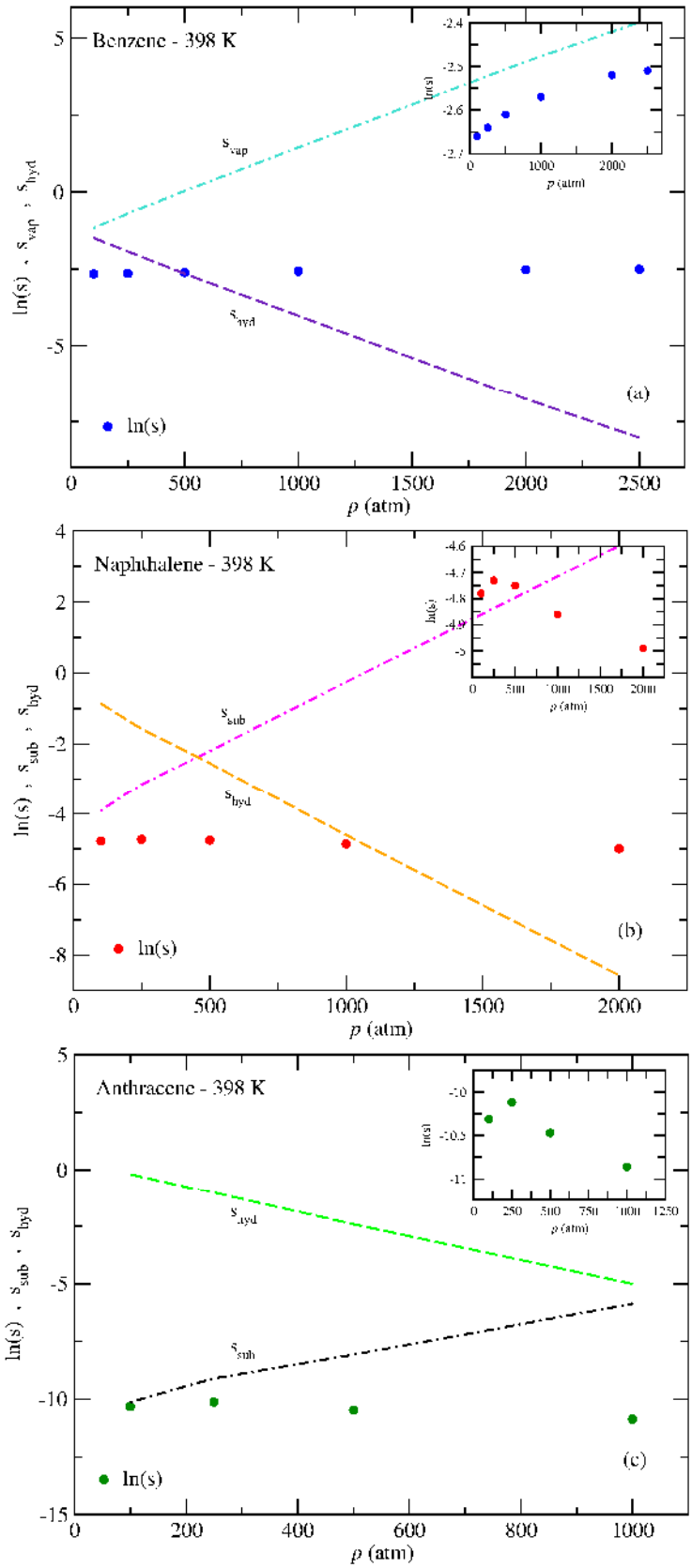

Figure 6 - Pressure dependence of the solubility of benzene, naphthalene, and anthracene at 398 K.

Thus, ΔG_{hyd} must increase via the decrease of $T\Delta S_{hyd}$, as expected, since the size of voids in the liquid is significantly reduced at high pressures. This increase of ΔG_{hyd} with pressure, may, therefore, be mapped, to some extent, to the dielectric constant increase, since the latter is closely related to the volume decrease and water-water interactions, also linked with the reduction of suitable voids in the liquid for solute insertion. However, it opposes the more intuitive view, associated to the DCP, where the increase of the dielectric constant leads to an increase (less negative) of the solute-water potential energy, for non-polar molecules, increasing ΔH_{hyd} and ΔG_{hyd}, and, therefore, reducing the solubility. The situation is similar to the decrease of ΔG_{hyd} above 475 K at 100 atm, contributing to the solubility increase, via the $T\Delta S_{hyd}$, rather than through a ΔH_{hyd} decrease (see Fig. 2).

Regarding gallic acid, the solubility increase in SBCW cannot be associated to the dielectric constant decrease of water, as previously discussed, since ΔG_{hyd} increases, and therefore, s_{hyd} decreases, with the temperature. The self-solvation free energy of gallic acid (see Fig. 6-SI), however, increases monotonically with the temperature, similar to the non-polar solutes, explaining the solubility increase in SBCW, observed experimentally. The ΔG_{self} values for gallic acid are significantly lower than for the non-polar solutes, leading to negligible vapor pressures (see eq. (6)) and, therefore, a negligible solubility, except at very high temperatures. Although no experimental vapor pressures are available for gallic acid, this suggests that the force field may not accurately describe the pure system. In spite a reasonable agreement was found between the density of the supercooled liquid at 298 K ($\rho \sim 1.510$ gcm^{-3}) and the experimental density of the solid ($\rho \sim 1.7$ gcm^{-3}), similar to the non-polar solutes, its accuracy with respect to standard thermodynamic properties such as the enthalpy of sublimation, often used to validate force fields, cannot be probed, since no experimental data is available. Another potential weakness concerns the higher saturation concentration for polar solutes, relative to sparklingly soluble solutes, thus, significantly deviating from infinite dilution. Nonetheless, the poor accuracy of the solubility as probed through eq.(8), does not change our conclusion regarding the role of the dielectric constant on the solubility of gallic acid.

C. Hydration Water Structure

We now turn attention to the structure of water next to the non-polar solutes, which has long been debated in connection to the negative hydration entropy[20], a hallmark of hydrophobic hydration. A possible negative entropic contribution at 298 K and 1 atm is connected to the view that water is more structured[30,31,36] (although very different from ice[20,138]) near hydrophobic solutes and groups, relative to bulk water. A positive entropic contribution has been related, instead, with a

large number of broken water-water HBs, observed next to large solutes, including benzene[31]. A structural enhancement was previously found for water molecules surrounded by four or more water neighbors (4MWN) in the first coordination sphere of benzene[31,139,140]. Here, we observe the same behavior both in the first and second HSh of benzene at 1 atm and 100 atm (see Fig. 7a); bulk water is defined as any water molecule at a distance larger than 15 Å from the solute center of mass (see Figs 4-SI and 5-SI). A similar enhancement was observed next to both naphthalene and anthracene, although for anthracene this is restricted to the second HSh (see Fig. 8-SI). Further, a decrease of the structural enhancement in the first and second HSh with the solute size is observed. This is expected in view of the decrease of the curvature of the molecular surface next to the shared C atoms of the aromatic rings, resulting in a larger number of broken HBs[24] and more distorted tetrahedrons, even for water molecules that retain four water neighbors. The structure of water was also assessed through the calculation of the local structure index (LSI) exhibiting a distribution similar to that observed for water at low temperatures[141,142], where a low density liquid (LDL) water population is more abundant (see Fig. 7b).

These observations contrast with those by Duboué-Dijon and Laage[38]. The reason is that the authors assume that every water molecule next to a hydrophobic solute "retains an intact first HSh containing four water neighbors". The latter, however, is a poor approximation as previously discussed (see Fig. 1-SI). Figure 9-SI shows the $P(O\cdots O_n)$ and the average $r_{O\cdots O_n}$ for n = 1 to 5, for the first and second HSh of benzene and bulk water, showing that the larger differences occur for the fourth and fifth nearest water neighbors. The latter are, therefore, beyond the first HSh, for some water molecules, disrupting tetrahedrality. Thus, by assessing the tetrahedrality of water molecules with L4WN an artificial decrease of the tetrahedrality is found. This has been previously observed[31,33,34] for different solutes, with a tetrahedrality enhancement starting at a distance from the solute, where water molecules have four water neighbors. Duboué-Dijon and Laage[38] found an increase of the LSI next to a hydrophobic solute consistent with that found here. This has been related to water depletion near the solute, leading to an artificial increase of the LSI. However, although the LSI is in general higher in low density environments, it does not necessarily increase upon water depletion. Thus, although water molecules with L4WN have a lower number of neighbors up to 3.7 Å, than water molecules with 4MWN, because of their proximity to the solute, a lower LSI value is found for molecules with 4MWN in the first HSh. Thus, while not probing the tetrahedrality, the LSI is consistent with q in that water next to a hydrophobic solute has resemblances to water at low temperatures. Furthermore, it has been shown that water molecules with less than 5 neighbors in the first HSh (r < 3.5 Å) are more tetrahedral (higher q) than water molecules with 5 neighbors, in pure model water[143]. Thus, water depletion, specifically, the lack of

interstitial water molecules, causes an increase of the tetrahedrality.

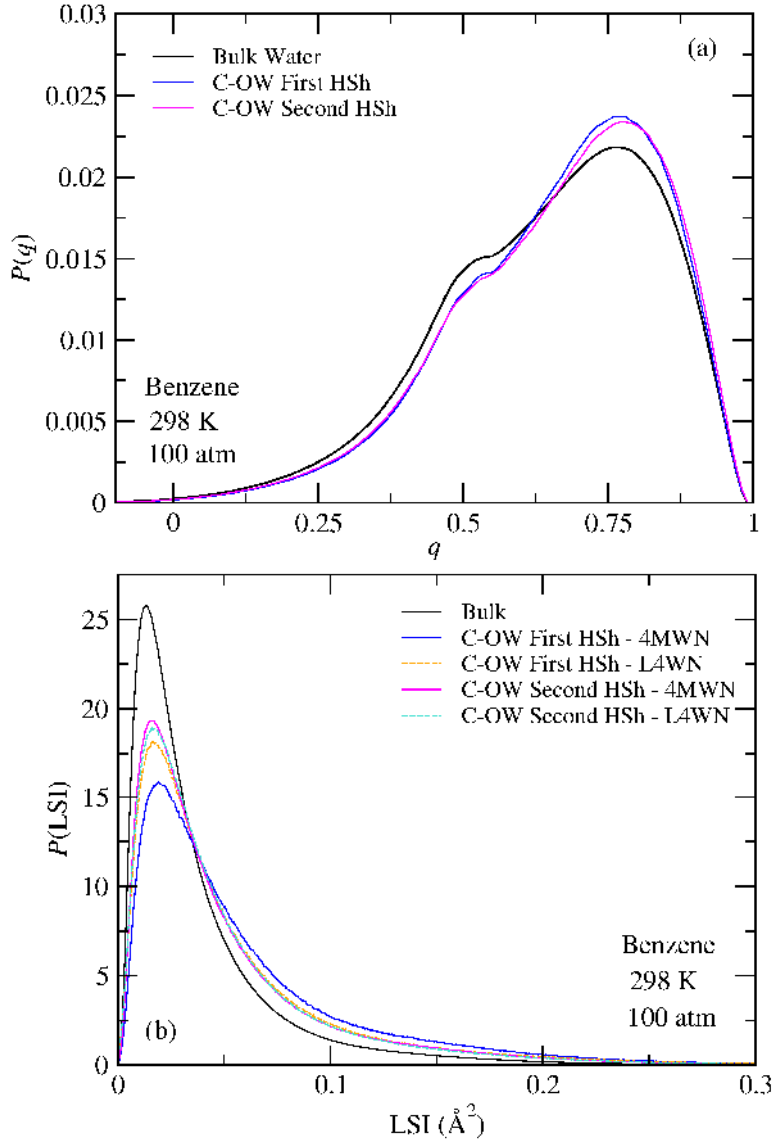

Figure 7 – (a) Tetrahedrality, q, of bulk water and water molecules with 4 or more water neighbors (4MWN) in the first and second hydration shells of the C atoms of benzene at 298 K and 100 atm. (b) LSI of bulk water and water molecules in the first and second hydration shells of the C atoms of benzene at 100 atm. The first hydration shell (HSh) is deconvoluted into water molecules with 4MWN and less than four water neighbors (L4WN). Water molecules in the HSh of more than one C atom are only counted once in the calculation of q and of the LSI. The 4MWN population represents 45% of the first HSh (N_w = 17.0) and 72% of the second HSh (N_w = 30.7). N_w is the number of distinct water molecules in the first and second HSh of the six C atoms of benzene and should not be confused with the coordination numbers, N_c. The LSI distributions at 1 atm are almost identical to the LSI distributions at 100 atm and are not shown.

Figure 8 shows the pair interaction energies between the nth (n = 1 to 4) nearest water neighbors in the bulk and in the first HSh of benzene at 298 K and 100 atm. As can be seen, the strongest interaction is found between a pair of nearest water neighbors (n = 1) in the HSh, for water molecules with L4WN. The pair interactions between the n = 1 to 4 neighbors for molecules with 4MWN are stronger than those found in bulk water. For n = 5 the pair interaction energy in the

bulk is stronger, instead, since the fifth neighbor already appears at a larger distance than in the bulk, because of the proximity of the solute (see Fig. 9-SI(d) and Tables 2-SI and 5-SI). For waters with L4WN, pair interactions are weaker than in the bulk for n > 2, for similar reasons. Thus, solute-water interactions replace water-water interactions for n > 2 in this water population. Interestingly, the tetrahedrality enhancement previously discussed in water molecules with 4MWN reflects especially in the pair interactions involving the third and fourth nearest neighbors, which are significantly stronger than in bulk water (see Figs 8(c) and (d)). Similar results were found in the second HSh (see Fig. 10-SI) as well as at 1 atm and at 378 K and 1 atm and 100 atm (see Tables SI-2 to SI-5).

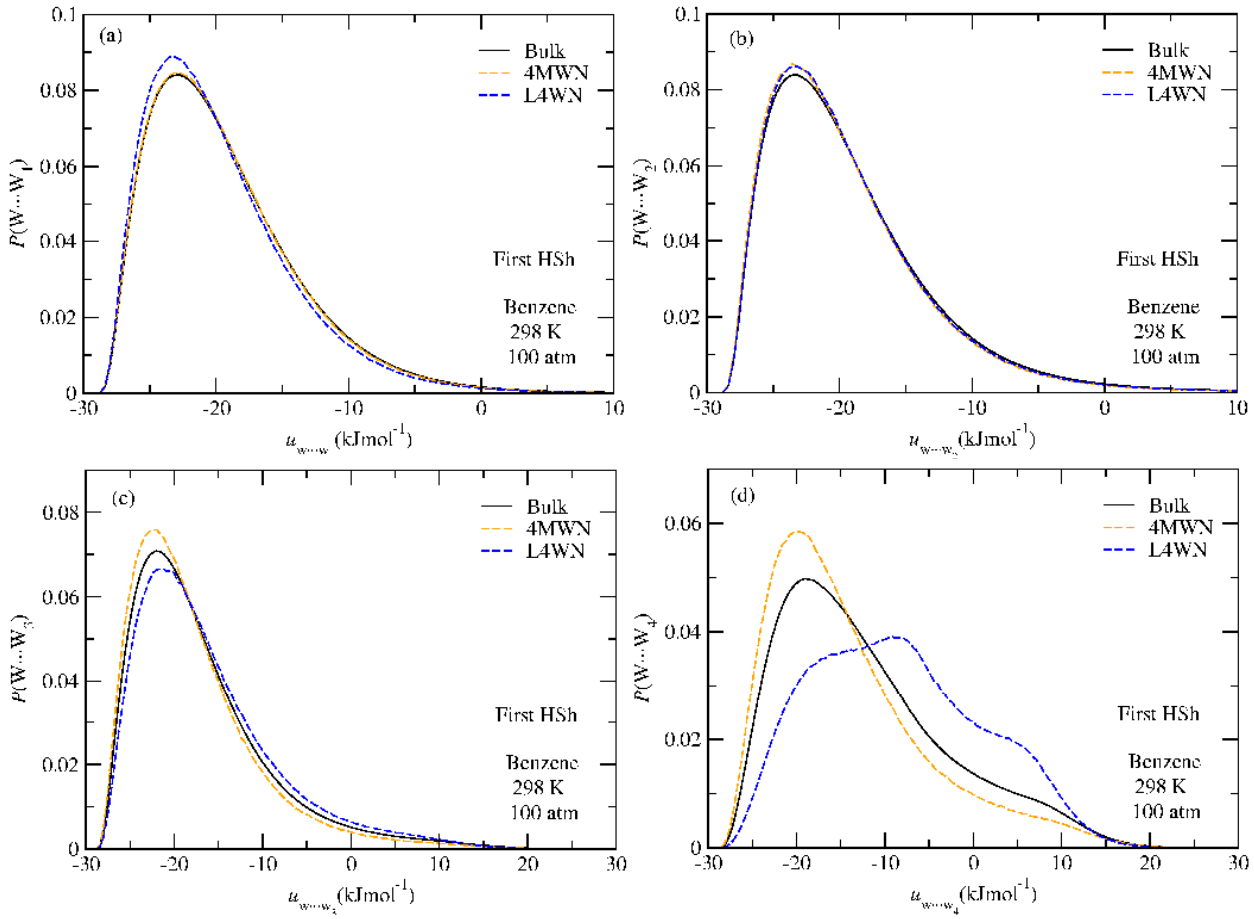

Figure 8 – Water pair interaction energy distributions, $P(W\cdots W_n)$ for n = 1 to 4, for bulk water and 4MWN and L4WN water populations in the first hydration shell of benzene at 298 K and 100 atm. The N_W with 4MWN and with L4WN is 7.5 and 9.3, respectively. Similar results were found for an aqueous solution at 1 atm; see Table 2-SI to 5-SI in the SI. The distributions for the 4MWN and L4WN in (b) are nearly indistinguishable.

Furthermore, in spite, of the differences previously discussed for the tetrahedrality of anthracene, stronger pair interactions were also found in the first (and second) HSh, for both naphthalene and

anthracene. The reason is that q does not probe the HB angle and distance, and shorter $r_{O\cdots O_n}$ (n = 1 to 4) as well as $r_{O\cdots H}$ (mean distance of an O atom to the nearest two H atoms of neighbor water molecules) are still observed in the first HSh of anthracene, relative to bulk water (see Fig. 11-SI).

The net balance between the stronger water-water interactions for water molecules with 4MWN (n ≤ 4) and with L4WN (n ≤ 2) and the weaker interactions for n = 5 and n > 2 for the 4MWN and L4WN populations, in the first and second HSh, and the solute-water interactions, cannot, however, be easily disentangled, Thus, although our results clearly show a structural enhancement and a lower interaction energy of some water pairs, relative to bulk water, contributing to the negative hydration enthalpy and entropy, the replacement of some water-water interactions (HBs) by solute-water interactions should exert the opposite effect. We recall that this entropic-enthalpic components, associated to the re-organization of water around the solutes, should nearly cancel, making a negligible contribution to the hydration free energy, and, therefore, to the hydration component of the solubility.

We also calculated the tetrahedrality and the pair interaction energies at 498 K, already above the temperature (~475 K) at which a nearly zero $T\Delta S_{hyd}$ is observed (see Fig. 3b) corresponding to the maximum of ΔG_{hyd}. At this temperature (see Fig. 12-SI) the structural and energetic enhancement previously discussed for the population comprised by water molecules with 4MWN, relative to bulk water, nearly vanishes, especially in the second HSh (see Fig. 9; similar results were found for naphthalene and anthracene). Although stronger water pair interactions are still observed in the first HSh for every solute, the number of water molecules with 4MWN in the first HSh at this temperature is much lower than the population with L4WN (see Fig. 13-SI for benzene; similar results were found for naphthalene and anthracene). These stronger water pair interactions in the first HSh, despite of a marginal tetrahedrality difference, relative to bulk water, result from the fact that significantly shorter $r_{O\cdots O_n}$ (n = 1 to 4) as well as $r_{O\cdots H}$ distances are still observed in the first HSh, opposite to the second HSh, where similar distances to those in bulk water are observed at this temperature.

These results indicate that while the water re-organization at room temperature may contribute to either a more negative or to a less negative $T\Delta S_{hyd}$, at high temperatures (T > 475K), this contribution should be positive, consistent with a positive $T\Delta S_{hyd}$ (see Fig. 3c), which should no longer be governed by the reversible work to form a cavity for solute insertion.

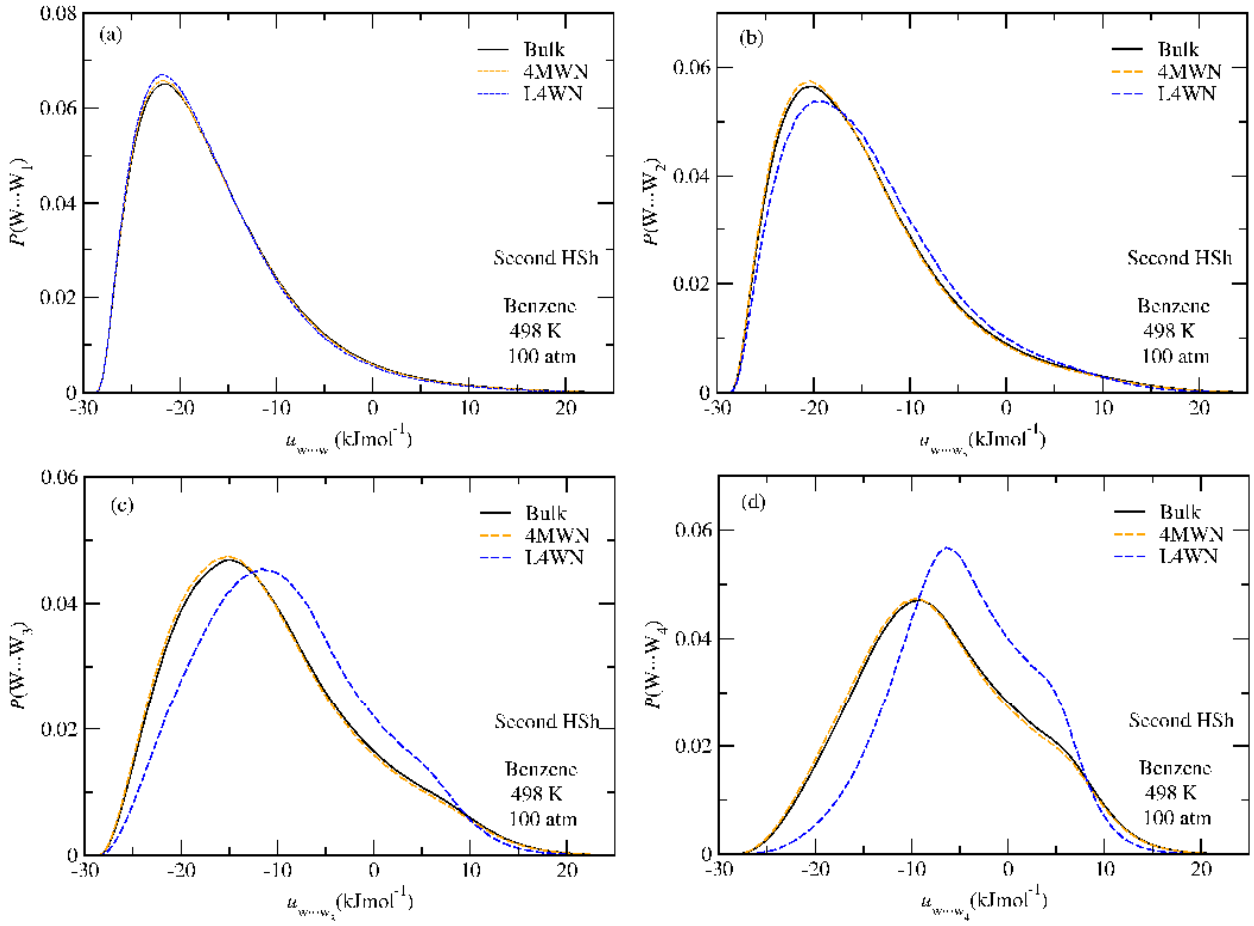

Figure 9 - Water pair interaction energy distributions, $P(W\cdots W_n)$, n = 1 to 4, for bulk water and 4MWN and L4WN water populations in the second hydration shell of benzene at 498 K and 100 atm. The N_W with 4MWN and with L4WN are 14.8 and 9.0, respectively.

With respect to the relationship between water-water interactions and the pressure dependence of the dielectric constant, Tables 2-SI to 5-SI, show a decrease of the water pair interactions in bulk water at 100 atm, relative to 1 atm, for n ≤ 4 and an increase for n = 5. This is expected, since the local orientational order (n ≤ 4) is reduced with the pressure increase, while the distance between a water molecule and its nth (n > 4) neighbors decreases, thus explaining the decrease of the water-water internal energy contribution with pressure. This is turn, along with the volume decrease, leads to an increase of the dielectric constant, and a decrease of the hydration component of the solubility, via $T\Delta S_{hyd}$.

IV. Conclusions

Subcritical water extraction is a green process allowing extracting polar and non-polar substances by varying only the temperature and pressure. The solubility increase of non-polar and some polar solutes in subcritical water has been commonly rationalized by the decrease of the

dielectric constant of water, whereas the solubility decrease at high pressures, has been associated to a moderate increase of the dielectric constant.

Here, we provide evidence from molecular dynamics simulations that this dielectric constant picture cannot account for the solubility increase in SBCW. Thus, we show that the solubility increase is related, instead, to the vaporization or sublimation components of the solubility of the pure liquid or solid solutes, respectively. The solubility increase of benzene and the solubility decrease of naphthalene and anthracene at high pressures, in turn, can be explained by the relative magnitude of the hydration and the vaporization or sublimation components of the solubility. Thus, in spite the dielectric constant picture is consistent with the increase of the hydration free energy and, therefore, with the decrease of the hydration component of the solubility with pressure, it cannot account for the pressure dependence of the solubility. Moreover the increase of the hydration component is not related to less favorable solute-water interactions but to the hydration entropy decrease, instead, associated to the volume decrease. Further, our results show that the solubility increase with the temperature of a model solid polar solute, such as gallic acid, in SBCW, is not related to the dielectric constant of water, but rather, with the increase of the sublimation component of the solubility.

Thus, while various models have been developed to predict the solubility of solids in subcritical water (see refs [3,15] and references therein), assuming a key role of the dielectric constant of water, our results contradict this picture, and show that while a description of the structural transformations of water at high temperatures is key, either through the dielectric constant or any empirical parameter, the latter contributes to a decrease, rather than to an increase, of the solubility of non-polar solutes.

Analysis of the structure of water shows that water molecules at room temperature, that retain four or more water neighbors next to the non-polar solutes are more ordered than bulk water, except for the first HSh of anthracene, significantly enhancing the interaction between a water molecule and its third and fourth nearest water neighbors. While these interactions should contribute to the negative hydration enthalpy and entropy, the net effect of this structural enhancement and the replacement of some water-water interactions by solute-water interactions, cannot be easily disentangled. This structural enhancement, in turn, nearly vanishes at high temperatures contributing to a positive hydration entropy. The latter, however, should not significantly contribute to the free energy and the solubility.

Acknowledgements

NG would like to acknowledge financial support from Fundação para a Ciência e a Tecnologia of

Portugal (SFRH/BPD/110483/2015). This work was supported by UID/MULTI/04046/2013 centre grant from FCT, Portugal (to BioISI) and by the Portuguese National Distributed Computing Infrastructure (http://www.incd.pt).

Supporting Information

Several figures and tables illustrating points discussed in text are available free of charge in the Supporting Information.

References

(1) Miller, D. J.; Hawthorne, S. B. Method for Determining the Solubilities of Hydrophobic Organics in Subcritical Water. *Anal. Chem.* **1998**, *70* (8), 1618–1621. https://doi.org/10.1021/ac971161x.

(2) Miller, D. J.; Hawthorne, S. B.; Gizir, A. M.; Clifford, A. A. Solubility of Polycyclic Aromatic Hydrocarbons in Subcritical Water from 298 K to 498 K. *J. Chem. Eng. Data* **1998**, *43* (6), 1043–1047. https://doi.org/10.1021/je980094g.

(3) Carr, A. G.; Mammucari, R.; Foster, N. R. A Review of Subcritical Water as a Solvent and Its Utilisation for the Processing of Hydrophobic Organic Compounds. *Chem. Eng. J.* **2011**, *172* (1), 1–17. https://doi.org/10.1016/j.cej.2011.06.007.

(4) Plaza, M.; Turner, C. Pressurized Hot Water Extraction of Bioactives. *TrAC Trends Anal. Chem.* **2015**, *71*, 39–54. https://doi.org/10.1016/j.trac.2015.02.022.

(5) Gbashi, S.; Adebo, O. A.; Piater, L.; Madala, N. E.; Njobeh, P. B. Subcritical Water Extraction of Biological Materials. *Sep. Purif. Rev.* **2017**, *46* (1), 21–34. https://doi.org/10.1080/15422119.2016.1170035.

(6) Liang, X.; Fan, Q. Application of Sub-Critical Water Extraction in Pharmaceutical Industry. *J. Mater. Sci. Chem. Eng.* **2013**, *01* (05), 1–6. https://doi.org/10.4236/msce.2013.15001.

(7) King, J. W. Pressurized Water Extraction: Resources and Techniques for Optimizing Analytical Applications. In *Modern Extraction Techniques*; Turner, C., Ed.; American Chemical Society: Washington, DC, 2006; Vol. 926, pp 79–95. https://doi.org/10.1021/bk-2006-0926.ch006.

(8) Curren, M. S. S.; King, J. W. Solubility of Triazine Pesticides in Pure and Modified Subcritical Water. *Anal. Chem.* **2001**, *73* (4), 740–745. https://doi.org/10.1021/ac000906n.

(9) Uematsu, M.; Frank, E. U. Static Dielectric Constant of Water and Steam. *J. Phys. Chem. Ref. Data* **1980**, *9* (4), 1291–1306. https://doi.org/10.1063/1.555632.

(10) Shirke, R. M.; Chaudhari, A.; More, N. M.; Patil, P. B. Temperature Dependent Dielectric Relaxation Study of Ethyl Acetate — Alcohol Mixtures Using Time Domain Technique. *J. Mol. Liq.* **2001**, *94* (1), 27–36. https://doi.org/10.1016/S0167-7322(01)00239-2.

(11) Miller, D. J.; Hawthorne, S. B. Solubility of Liquid Organic Flavor and Fragrance Compounds in Subcritical (Hot/Liquid) Water from 298 K to 473 K. *J. Chem. Eng. Data* **2000**, *45* (2), 315–318. https://doi.org/10.1021/je990278a.

(12) Srinivas, K.; King, J. W.; Howard, L. R.; Monrad, J. K. Solubility of Gallic Acid, Catechin, and Protocatechuic Acid in Subcritical Water from (298.75 to 415.85) K. *J. Chem. Eng. Data* **2010**, *55* (9), 3101–3108. https://doi.org/10.1021/je901097n.

(13) Teoh, W. H.; Mammucari, R.; Vieira de Melo, S. A. B.; Foster, N. R. Solubility and Solubility Modeling of Polycyclic Aromatic Hydrocarbons in Subcritical Water. *Ind. Eng. Chem. Res.* **2013**, *52* (16), 5806–5814. https://doi.org/10.1021/ie302124e.

(14) Sawamura, S.; Nagaoka, K.; Machikawa, T. Effects of Pressure and Temperature on the Solubility of Alkylbenzenes in Water: Volumetric Property of Hydrophobic Hydration. *J. Phys. Chem. B* **2001**, *105* (12), 2429–2436. https://doi.org/10.1021/jp0021953.

(15) Fornari, T.; Stateva, R. P.; Señorans, F. J.; Reglero, G.; Ibañez, E. Applying UNIFAC-Based Models to Predict the Solubility of Solids in Subcritical Water. *J. Supercrit. Fluids* **2008**, *46* (3), 245–251. https://doi.org/10.1016/j.supflu.2007.11.017.
(16) Carr, A. G.; Branch, A.; Mammucari, R.; Foster, N. R. The Solubility and Solubility Modelling of Budesonide in Pure and Modified Subcritical Water Solutions. *J. Supercrit. Fluids* **2010**, *55* (1), 37–42. https://doi.org/10.1016/j.supflu.2010.08.001.
(17) Hansen, C. M. *Hansen Solubility Parameters: A User's Handbook*, 2nd ed.; CRC Press: Boca Raton, 2007.
(18) Pollack, G. L. Why Gases Dissolve in Liquids. *Science* **1991**, *251* (4999), 1323–1330. https://doi.org/10.1126/science.251.4999.1323.
(19) Prini, R. F.; Crovetto, R. Evaluation of Data on Solubility of Simple Apolar Gases in Light and Heavy Water at High Temperature. *J. Phys. Chem. Ref. Data* **1989**, *18* (3), 1231–1243. https://doi.org/10.1063/1.555834.
(20) Frank, H. S.; Evans, M. W. Free Volume and Entropy in Condensed Systems III. Entropy in Binary Liquid Mixtures; Partial Molal Entropy in Dilute Solutions; Structure and Thermodynamics in Aqueous Electrolytes. *J. Chem. Phys.* **1945**, *13* (11), 507. https://doi.org/10.1063/1.1723985.
(21) Makhatadze, G. I.; Privalov, P. L. Energetics of Interactions of Aromatic Hydrocarbons with Water. *Biophys. Chem.* **1994**, *50* (3), 285–291. https://doi.org/10.1016/0301-4622(93)E0096-N.
(22) Lum, K.; Chandler, D.; Weeks, J. D. Hydrophobicity at Small and Large Length Scales. *J. Phys. Chem. B* **1999**, *103* (22), 4570–4577. https://doi.org/10.1021/jp984327m.
(23) Hummer, G.; Garde, S.; Garcia, A. E.; Pohorille, A.; Pratt, L. R. An Information Theory Model of Hydrophobic Interactions. *Proc. Natl. Acad. Sci.* **1996**, *93* (17), 8951.
(24) Chandler, D. Interfaces and the Driving Force of Hydrophobic Assembly. *Nature* **2005**, *437* (7059), 640–647. https://doi.org/10.1038/nature04162.
(25) Graziano, G. On the Size Dependence of Hydrophobic Hydration. *J. Chem. Soc. Faraday Trans.* **1998**, *94* (22), 3345–3352. https://doi.org/10.1039/a805733h.
(26) Guillot, B.; Guissani, Y. A Computer Simulation Study of the Temperature Dependence of the Hydrophobic Hydration. *J. Chem. Phys.* **1993**, *99* (10), 8075–8094. https://doi.org/10.1063/1.465634.
(27) Garde, S.; García, A. E.; Pratt, L. R.; Hummer, G. Temperature Dependence of the Solubility of Non-Polar Gases in Water. *Biophys. Chem.* **1999**, *78* (1–2), 21–32. https://doi.org/10.1016/S0301-4622(99)00018-6.
(28) Gallicchio, E.; Kubo, M. M.; Levy, R. M. Enthalpy−Entropy and Cavity Decomposition of Alkane Hydration Free Energies: Numerical Results and Implications for Theories of Hydrophobic Solvation. *J. Phys. Chem. B* **2000**, *104* (26), 6271–6285. https://doi.org/10.1021/jp0006274.
(29) Southall, N. T.; Dill, K. A.; Haymet, A. D. J. A View of the Hydrophobic Effect. *J. Phys. Chem. B* **2002**, *106* (3), 521–533. https://doi.org/10.1021/jp015514e.
(30) Davis, J. G.; Gierszal, K. P.; Wang, P.; Ben-Amotz, D. Water Structural Transformation at Molecular Hydrophobic Interfaces. *Nature* **2012**, *491* (7425), 582–585. https://doi.org/10.1038/nature11570.
(31) Galamba, N. Water's Structure around Hydrophobic Solutes and the Iceberg Model. *J. Phys. Chem. B* **2013**, *117* (7), 2153–2159. https://doi.org/10.1021/jp310649n.
(32) Martiniano, H. F. M. C.; Galamba, N. Fast and Slow Dynamics and the Local Structure of Liquid and Supercooled Water next to a Hydrophobic Amino Acid. *Phys Chem Chem Phys* **2016**, *18* (39), 27639–27647. https://doi.org/10.1039/C6CP04532D.
(33) Song, B.; Molinero, V. Thermodynamic and Structural Signatures of Water-Driven Methane-Methane Attraction in Coarse-Grained MW Water. *J. Chem. Phys.* **2013**, *139* (5), 054511. https://doi.org/10.1063/1.4816005.
(34) Ashbaugh, H. S.; Barnett, J. W.; Saltzman, A.; Langrehr, M. E.; Houser, H. Communication:

Stiffening of Dilute Alcohol and Alkane Mixtures with Water. *J. Chem. Phys.* **2016**, *145* (20), 201102. https://doi.org/10.1063/1.4971205.
(35) Daschakraborty, S. How Do Glycerol and Dimethyl Sulphoxide Affect Local Tetrahedral Structure of Water around a Nonpolar Solute at Low Temperature? Importance of Preferential Interaction. *J. Chem. Phys.* **2018**, *148* (13), 134501. https://doi.org/10.1063/1.5019239.
(36) Galamba, N. Reply to "Comment on 'Water's Structure around Hydrophobic Solutes and the Iceberg Model.'" *J. Phys. Chem. B* **2014**, *118* (9), 2600–2603. https://doi.org/10.1021/jp501450n.
(37) Buchanan, P.; Aldiwan, N.; Soper, A. K.; Creek, J. L.; Koh, C. A. Decreased Structure on Dissolving Methane in Water. *Chem. Phys. Lett.* **2005**, *415* (1–3), 89–93. https://doi.org/10.1016/j.cplett.2005.08.064.
(38) Duboué-Dijon, E.; Laage, D. Characterization of the Local Structure in Liquid Water by Various Order Parameters. *J. Phys. Chem. B* **2015**, *119* (26), 8406–8418. https://doi.org/10.1021/acs.jpcb.5b02936.
(39) Turner, J.; Soper, A. K. The Effect of Apolar Solutes on Water Structure: Alcohols and Tetraalkylammonium Ions. *J. Chem. Phys.* **1994**, *101* (7), 6116. https://doi.org/10.1063/1.467327.
(40) Graziano, G. Comment on "Water's Structure around Hydrophobic Solutes and the Iceberg Model." *J. Phys. Chem. B* **2014**, *118* (9), 2598–2599. https://doi.org/10.1021/jp5008895.
(41) Ben-Naim, A. Hydrophobic Interaction and Structural Changes in the Solvent. *Biopolymers* **1975**, *14* (7), 1337–1355. https://doi.org/10.1002/bip.1975.360140704.
(42) Yu, H.-A.; Karplus, M. A Thermodynamic Analysis of Solvation. *J. Chem. Phys.* **1988**, *89* (4), 2366. https://doi.org/10.1063/1.455080.
(43) Lee, B. Solvent Reorganization Contribution to the Transfer Thermodynamics of Small Nonpolar Molecules. *Biopolymers* **1991**, *31* (8), 993–1008. https://doi.org/10.1002/bip.360310809.
(44) Grunwald, E.; Steel, C. Solvent Reorganization and Thermodynamic Enthalpy-Entropy Compensation. *J. Am. Chem. Soc.* **1995**, *117* (21), 5687–5692. https://doi.org/10.1021/ja00126a009.
(45) Qian, H.; Hopfield, J. J. Entropy-Enthalpy Compensation: Perturbation and Relaxation in Thermodynamic Systems. *J. Chem. Phys.* **1996**, *105* (20), 9292. https://doi.org/10.1063/1.472728.
(46) Ben-Amotz, D.; Underwood, R. Unraveling Water's Entropic Mysteries: A Unified View of Nonpolar, Polar, and Ionic Hydration. *Acc. Chem. Res.* **2008**, *41* (8), 957–967. https://doi.org/10.1021/ar7001478.
(47) Ben-Naim, A. A Simple Model for Demonstrating the Relation between Solubility, Hydrophobic Interaction, and Structural Changes in the Solvent. *J. Phys. Chem.* **1978**, *82* (8), 874–885. https://doi.org/10.1021/j100497a007.
(48) Graziano, G.; Lee, B. Hydration of Aromatic Hydrocarbons. *J. Phys. Chem. B* **2001**, *105* (42), 10367–10372. https://doi.org/10.1021/jp011382d.
(49) Schravendijk, P.; van der Vegt, N. F. A. From Hydrophobic to Hydrophilic Solvation: An Application to Hydration of Benzene. *J. Chem. Theory Comput.* **2005**, *1* (4), 643–652. https://doi.org/10.1021/ct049841c.
(50) Mordasini Denti, T. Z.; Beutler, T. C.; van Gunsteren, W. F.; Diederich, F. Computation of Gibbs Free Energies of Hydration for Simple Aromatic Molecules: A Comparative Study Using Monte Carlo and Molecular Dynamics Computer Simulation Techniques. *J. Phys. Chem.* **1996**, *100* (10), 4256–4260. https://doi.org/10.1021/jp9525797.
(51) Graziano, G. Benzene Solubility in Water: A Reassessment. *Chem. Phys. Lett.* **2006**, *429* (1–3), 114–118. https://doi.org/10.1016/j.cplett.2006.08.006.
(52) Bohon, R. L.; Claussen, W. F. The Solubility of Aromatic Hydrocarbons in Water. *J. Am. Chem. Soc.* **1951**, *73* (4), 1571–1578. https://doi.org/10.1021/ja01148a047.

(53) Andersson, T. A.; Hartonen, K. M.; Riekkola, M.-L. Solubility of Acenaphthene, Anthracene, and Pyrene in Water At 50 °C to 300 °C. *J. Chem. Eng. Data* **2005**, *50* (4), 1177–1183. https://doi.org/10.1021/je0495886.
(54) Thompson, J. D.; Cramer, C. J.; Truhlar, D. G. Predicting Aqueous Solubilities from Aqueous Free Energies of Solvation and Experimental or Calculated Vapor Pressures of Pure Substances. *J. Chem. Phys.* **2003**, *119* (3), 1661–1670. https://doi.org/10.1063/1.1579474.
(55) Ahmed, A.; Sandler, S. I. Physicochemical Properties of Hazardous Energetic Compounds from Molecular Simulation. *J. Chem. Theory Comput.* **2013**, *9* (5), 2389–2397. https://doi.org/10.1021/ct301129x.
(56) Espinosa, J. R.; Young, J. M.; Jiang, H.; Gupta, D.; Vega, C.; Sanz, E.; Debenedetti, P. G.; Panagiotopoulos, A. Z. On the Calculation of Solubilities via Direct Coexistence Simulations: Investigation of NaCl Aqueous Solutions and Lennard-Jones Binary Mixtures. *J. Chem. Phys.* **2016**, *145* (15), 154111. https://doi.org/10.1063/1.4964725.
(57) Ferrario, M.; Ciccotti, G.; Spohr, E.; Cartailler, T.; Turq, P. Solubility of KF in Water by Molecular Dynamics Using the Kirkwood Integration Method. *J. Chem. Phys.* **2002**, *117* (10), 4947–4953. https://doi.org/10.1063/1.1498820.
(58) Schnieders, M. J.; Baltrusaitis, J.; Shi, Y.; Chattree, G.; Zheng, L.; Yang, W.; Ren, P. The Structure, Thermodynamics, and Solubility of Organic Crystals from Simulation with a Polarizable Force Field. *J. Chem. Theory Comput.* **2012**, *8* (5), 1721–1736. https://doi.org/10.1021/ct300035u.
(59) Palmer, D. S.; McDonagh, J. L.; Mitchell, J. B. O.; van Mourik, T.; Fedorov, M. V. First-Principles Calculation of the Intrinsic Aqueous Solubility of Crystalline Druglike Molecules. *J. Chem. Theory Comput.* **2012**, *8* (9), 3322–3337. https://doi.org/10.1021/ct300345m.
(60) Lüder, K.; Lindfors, L.; Westergren, J.; Nordholm, S.; Kjellander, R. In Silico Prediction of Drug Solubility: 2. Free Energy of Solvation in Pure Melts. *J. Phys. Chem. B* **2007**, *111* (7), 1883–1892. https://doi.org/10.1021/jp0642239.
(61) Manzanilla-Granados, H. M.; Saint-Martín, H.; Fuentes-Azcatl, R.; Alejandre, J. Direct Coexistence Methods to Determine the Solubility of Salts in Water from Numerical Simulations. Test Case NaCl. *J. Phys. Chem. B* **2015**, *119* (26), 8389–8396. https://doi.org/10.1021/acs.jpcb.5b00740.
(62) Paluch, A. S.; Jayaraman, S.; Shah, J. K.; Maginn, E. J. A Method for Computing the Solubility Limit of Solids: Application to Sodium Chloride in Water and Alcohols. *J. Chem. Phys.* **2010**, *133* (12), 124504. https://doi.org/10.1063/1.3478539.
(63) Benavides, A. L.; Aragones, J. L.; Vega, C. Consensus on the Solubility of NaCl in Water from Computer Simulations Using the Chemical Potential Route. *J. Chem. Phys.* **2016**, *144* (12), 124504. https://doi.org/10.1063/1.4943780.
(64) Li, L.; Totton, T.; Frenkel, D. Computational Methodology for Solubility Prediction: Application to the Sparingly Soluble Solutes. *J. Chem. Phys.* **2017**, *146* (21), 214110. https://doi.org/10.1063/1.4983754.
(65) Ben-Naim, A. Standard Thermodynamics of Transfer. Uses and Misuses. *J. Phys. Chem.* **1978**, *82* (7), 792–803. https://doi.org/10.1021/j100496a008.
(66) Ahmed, A.; Sandler, S. I. Temperature-Dependent Physicochemical Properties and Solvation Thermodynamics of Nitrotoluenes from Solvation Free Energies. *J. Chem. Eng. Data* **2015**, *60* (1), 16–27. https://doi.org/10.1021/je500413a.
(67) Ahmed, A.; Sandler, S. I. Predictions of the Physicochemical Properties of Amino Acid Side Chain Analogs Using Molecular Simulation. *Phys. Chem. Chem. Phys.* **2016**, *18* (9), 6559–6568. https://doi.org/10.1039/C5CP05393E.
(68) Winget, P.; Hawkins, G. D.; Cramer, C. J.; Truhlar, D. G. Prediction of Vapor Pressures from Self-Solvation Free Energies Calculated by the SM5 Series of Universal Solvation Models. *J. Phys. Chem. B* **2000**, *104* (19), 4726–4734. https://doi.org/10.1021/jp992435i.

(69) Linstrom, P.; Mallard, W. *NIST Chemistry WebBook, NIST Standard Reference Database Number 69*; 2005.
(70) Acree, W.; Chickos, J. S. Phase Transition Enthalpy Measurements of Organic and Organometallic Compounds. Sublimation, Vaporization and Fusion Enthalpies From 1880 to 2015. Part 1. $C_1 - C_{10}$. *J. Phys. Chem. Ref. Data* **2016**, *45* (3), 033101. https://doi.org/10.1063/1.4948363.
(71) Bogel-Łukasik, R.; Nobre Gonçalves, L. M.; Bogel-Łukasik, E. Phase Equilibrium Phenomena in Solutions Involving Tannins, Flavonoids and Ionic Liquids. *Green Chem.* **2010**, *12* (11), 1947. https://doi.org/10.1039/c0gc00308e.
(72) Mota, F. L.; Queimada, A. J.; Pinho, S. P.; Macedo, E. A. Aqueous Solubility of Some Natural Phenolic Compounds. *Ind. Eng. Chem. Res.* **2008**, *47* (15), 5182–5189. https://doi.org/10.1021/ie071452o.
(73) Wang, J.; Wolf, R. M.; Caldwell, J. W.; Kollman, P. A.; Case, D. A. Development and Testing of a General Amber Force Field. *J. Comput. Chem.* **2004**, *25* (9), 1157–1174. https://doi.org/10.1002/jcc.20035.
(74) Horn, H. W.; Swope, W. C.; Pitera, J. W.; Madura, J. D.; Dick, T. J.; Hura, G. L.; Head-Gordon, T. Development of an Improved Four-Site Water Model for Biomolecular Simulations: TIP4P-Ew. *J. Chem. Phys.* **2004**, *120* (20), 9665. https://doi.org/10.1063/1.1683075.
(75) Daneshfar, A.; Ghaziaskar, H. S.; Homayoun, N. Solubility of Gallic Acid in Methanol, Ethanol, Water, and Ethyl Acetate. *J. Chem. Eng. Data* **2008**, *53* (3), 776–778. https://doi.org/10.1021/je700633w.
(76) Lu, L.-L.; Lu, X.-Y. Solubilities of Gallic Acid and Its Esters in Water. *J. Chem. Eng. Data* **2007**, *52* (1), 37–39. https://doi.org/10.1021/je0601661.
(77) Møller, Chr.; Plesset, M. S. Note on an Approximation Treatment for Many-Electron Systems. *Phys. Rev.* **1934**, *46* (7), 618–622. https://doi.org/10.1103/PhysRev.46.618.
(78) Dunning, T. H. Gaussian Basis Sets for Use in Correlated Molecular Calculations. I. The Atoms Boron through Neon and Hydrogen. *J. Chem. Phys.* **1989**, *90* (2), 1007–1023. https://doi.org/10.1063/1.456153.
(79) Besler, B. H.; Merz, K. M.; Kollman, P. A. Atomic Charges Derived from Semiempirical Methods. *J. Comput. Chem.* **1990**, *11* (4), 431–439. https://doi.org/10.1002/jcc.540110404.
(80) Singh, U. C.; Kollman, P. A. An Approach to Computing Electrostatic Charges for Molecules. *J. Comput. Chem.* **1984**, *5* (2), 129–145. https://doi.org/10.1002/jcc.540050204.
(81) M. J. Frisch, G. W. Trucks, H. B. Schlegel, G. E. Scuseria, M. A. Robb, J. R. Cheeseman, G. Scalmani, V. Barone, G. A. Petersson, H. Nakatsuji, X. Li, M. Caricato, A. Marenich, J. Bloino, B. G. Janesko, R. Gomperts, B. Mennucci, H. P. Hratchian, J. V. Ortiz, A. F. Izmaylov, J. L. Sonnenberg, D. Williams-Young, F. Ding, F. Lipparini, F. Egidi, J. Goings, B. Peng, A. Petrone, T. Henderson, D. Ranasinghe, V. G. Zakrzewski, J. Gao, N. Rega, G. Zheng, W. Liang, M. Hada, M. Ehara, K. Toyota, R. Fukuda, J. Hasegawa, M. Ishida, T. Nakajima, Y. Honda, O. Kitao, H. Nakai, T. Vreven, K. Throssell, J. A. Montgomery, Jr., J. E. Peralta, F. Ogliaro, M. Bearpark, J. J. Heyd, E. Brothers, K. N. Kudin, V. N. Staroverov, T. Keith, R. Kobayashi, J. Normand, K. Raghavachari, A. Rendell, J. C. Burant, S. S. Iyengar, J. Tomasi, M. Cossi, J. M. Millam, M. Klene, C. Adamo, R. Cammi, J. W. Ochterski, R. L. Martin, K. Morokuma, O. Farkas, J. B. Foresman, and D. J. Fox,. *Gaussian 09. Revision D.01*; Gaussian, Inc.: Wallingford CT, 2016.
(82) Hohenberg, P.; Kohn, W. Inhomogeneous Electron Gas. *Phys. Rev.* **1964**, *136* (3B), B864–B871. https://doi.org/10.1103/PhysRev.136.B864.
(83) Kohn, W.; Sham, L. J. Self-Consistent Equations Including Exchange and Correlation Effects. *Phys. Rev.* **1965**, *140* (4A), A1133–A1138. https://doi.org/10.1103/PhysRev.140.A1133.
(84) Lee, C.; Yang, W.; Parr, R. G. Development of the Colle-Salvetti Correlation-Energy Formula into a Functional of the Electron Density. *Phys. Rev. B* **1988**, *37* (2), 785–789.

https://doi.org/10.1103/PhysRevB.37.785.
(85) Becke, A. D. Density-functional Thermochemistry. III. The Role of Exact Exchange. *J. Chem. Phys.* **1993**, *98* (7), 5648–5652. https://doi.org/10.1063/1.464913.
(86) Cornell, W. D.; Cieplak, P.; Bayly, C. I.; Kollman, P. A. Application of RESP Charges to Calculate Conformational Energies, Hydrogen Bond Energies, and Free Energies of Solvation. *J. Am. Chem. Soc.* **1993**, *115* (21), 9620–9631. https://doi.org/10.1021/ja00074a030.
(87) Jorgensen, W. L.; Chandrasekhar, J.; Madura, J. D.; Impey, R. W.; Klein, M. L. Comparison of Simple Potential Functions for Simulating Liquid Water. *J. Chem. Phys.* **1983**, *79* (2), 926–935. https://doi.org/10.1063/1.445869.
(88) Jorgensen, W. L.; Maxwell, D. S.; Tirado-Rives, J. Development and Testing of the OPLS All-Atom Force Field on Conformational Energetics and Properties of Organic Liquids. *J. Am. Chem. Soc.* **1996**, *118* (45), 11225–11236. https://doi.org/10.1021/ja9621760.
(89) Van Der Spoel, D.; Lindahl, E.; Hess, B.; Groenhof, G.; Mark, A. E.; Berendsen, H. J. C. GROMACS: Fast, Flexible, and Free. *J. Comput. Chem.* **2005**, *26* (16), 1701–1718. https://doi.org/10.1002/jcc.20291.
(90) Bussi, G.; Donadio, D.; Parrinello, M. Canonical Sampling through Velocity Rescaling. *J. Chem. Phys.* **2007**, *126* (1), 014101. https://doi.org/10.1063/1.2408420.
(91) Parrinello, M. Polymorphic Transitions in Single Crystals: A New Molecular Dynamics Method. *J. Appl. Phys.* **1981**, *52* (12), 7182. https://doi.org/10.1063/1.328693.
(92) Essmann, U.; Perera, L.; Berkowitz, M. L.; Darden, T.; Lee, H.; Pedersen, L. G. A Smooth Particle Mesh Ewald Method. *J. Chem. Phys.* **1995**, *103* (19), 8577. https://doi.org/10.1063/1.470117.
(93) Hess, B.; Bekker, H.; Berendsen, H. J. C.; Fraaije, J. G. E. M. LINCS: A Linear Constraint Solver for Molecular Simulations. *J. Comput. Chem.* **1997**, *18* (12), 1463–1472. https://doi.org/10.1002/(SICI)1096-987X(199709)18:12<1463::AID-JCC4>3.0.CO;2-H.
(94) Kirkwood, J. G. Statistical Mechanics of Fluid Mixtures. *J. Chem. Phys.* **1935**, *3* (5), 300–313. https://doi.org/10.1063/1.1749657.
(95) Zwanzig, R. W. High-Temperature Equation of State by a Perturbation Method. I. Nonpolar Gases. *J. Chem. Phys.* **1954**, *22* (8), 1420–1426. https://doi.org/10.1063/1.1740409.
(96) Duarte Ramos Matos, G.; Kyu, D. Y.; Loeffler, H. H.; Chodera, J. D.; Shirts, M. R.; Mobley, D. L. Approaches for Calculating Solvation Free Energies and Enthalpies Demonstrated with an Update of the FreeSolv Database. *J. Chem. Eng. Data* **2017**, *62* (5), 1559–1569. https://doi.org/10.1021/acs.jced.7b00104.
(97) Christ, C. D.; Mark, A. E.; van Gunsteren, W. F. Basic Ingredients of Free Energy Calculations: A Review. *J. Comput. Chem.* **2009**, NA-NA. https://doi.org/10.1002/jcc.21450.
(98) Pohorille, A.; Jarzynski, C.; Chipot, C. Good Practices in Free-Energy Calculations. *J. Phys. Chem. B* **2010**, *114* (32), 10235–10253. https://doi.org/10.1021/jp102971x.
(99) Bennett, C. H. Efficient Estimation of Free Energy Differences from Monte Carlo Data. *J. Comput. Phys.* **1976**, *22* (2), 245–268. https://doi.org/10.1016/0021-9991(76)90078-4.
(100) Van Gunsteren, W. F.; Berendsen, H. J. C. A Leap-Frog Algorithm for Stochastic Dynamics. *Mol. Simul.* **1988**, *1* (3), 173–185. https://doi.org/10.1080/08927028808080941.
(101) Steinbrecher, T.; Joung, I.; Case, D. A. Soft-Core Potentials in Thermodynamic Integration: Comparing One- and Two-Step Transformations. *J. Comput. Chem.* **2011**, *32* (15), 3253–3263. https://doi.org/10.1002/jcc.21909.
(102) Beutler, T. C.; Mark, A. E.; van Schaik, R. C.; Gerber, P. R.; van Gunsteren, W. F. Avoiding Singularities and Numerical Instabilities in Free Energy Calculations Based on Molecular Simulations. *Chem. Phys. Lett.* **1994**, *222* (6), 529–539. https://doi.org/10.1016/0009-2614(94)00397-1.
(103) Gapsys, V.; Seeliger, D.; de Groot, B. L. New Soft-Core Potential Function for Molecular Dynamics Based Alchemical Free Energy Calculations. *J. Chem. Theory Comput.* **2012**, *8*

(7), 2373–2382. https://doi.org/10.1021/ct300220p.
(104) Pham, T. T.; Shirts, M. R. Identifying Low Variance Pathways for Free Energy Calculations of Molecular Transformations in Solution Phase. *J. Chem. Phys.* **2011**, *135* (3), 034114. https://doi.org/10.1063/1.3607597.
(105) Levy, R. M.; Gallicchio, E. Computer Simulations with Explicit Solvent: Recent Progress in the Thermodynamic Decomposition of Free Energies and in Modeling Electrostatic Effects. *Annu. Rev. Phys. Chem.* **1998**, *49*, 531–567. https://doi.org/10.1146/annurev.physchem.49.1.531.
(106) Badyal, Y. S.; Saboungi, M.-L.; Price, D. L.; Shastri, S. D.; Haeffner, D. R.; Soper, A. K. Electron Distribution in Water. *J. Chem. Phys.* **2000**, *112* (21), 9206–9208. https://doi.org/10.1063/1.481541.
(107) Coulson, A. C.; Eisenberg, D. Interactions of H $_2$ O Molecules in Ice I. The Dipole Moment of an H $_2$ O Molecule in Ice. *Proc. R. Soc. Lond. Ser. Math. Phys. Sci.* **1966**, *291* (1427), 445–453. https://doi.org/10.1098/rspa.1966.0105.
(108) Gubskaya, A. V.; Kusalik, P. G. The Total Molecular Dipole Moment for Liquid Water. *J. Chem. Phys.* **2002**, *117* (11), 5290–5302. https://doi.org/10.1063/1.1501122.
(109) Silvestrelli, P. L.; Parrinello, M. Water Molecule Dipole in the Gas and in the Liquid Phase. *Phys. Rev. Lett.* **1999**, *82* (16), 3308–3311. https://doi.org/10.1103/PhysRevLett.82.3308.
(110) Site, L. D.; Alavi, A.; Lynden-Bell, R. M. The Electrostatic Properties of Water Molecules in Condensed Phases: An Ab Initio Study. *Mol. Phys.* **1999**, *96* (11), 1683–1693. https://doi.org/10.1080/00268979909483112.
(111) McGrath, M. J.; Siepmann, J. I.; Kuo, I.-F. W.; Mundy, C. J. Spatial Correlation of Dipole Fluctuations in Liquid Water. *Mol. Phys.* **2007**, *105* (10), 1411–1417. https://doi.org/10.1080/00268970701364938.
(112) Gregory, null; Clary, null; Liu, null; Brown, null; Saykally, null. The Water Dipole Moment in Water Clusters. *Science* **1997**, *275* (5301), 814–817.
(113) Kemp, D. D.; Gordon, M. S. An Interpretation of the Enhancement of the Water Dipole Moment Due to the Presence of Other Water Molecules. *J. Phys. Chem. A* **2008**, *112* (22), 4885–4894. https://doi.org/10.1021/jp801921f.
(114) Galamba, N.; Cabral, B. J. C. The Changing Hydrogen-Bond Network of Water from the Bulk to the Surface of a Cluster: A Born−Oppenheimer Molecular Dynamics Study. *J. Am. Chem. Soc.* **2008**, *130* (52), 17955–17960. https://doi.org/10.1021/ja807111y.
(115) Tu, Y.; Laaksonen, A. The Electronic Properties of Water Molecules in Water Clusters and Liquid Water. *Chem. Phys. Lett.* **2000**, *329* (3–4), 283–288. https://doi.org/10.1016/S0009-2614(00)01026-5.
(116) Kuo, I.-F. W. An Ab Initio Molecular Dynamics Study of the Aqueous Liquid-Vapor Interface. *Science* **2004**, *303* (5658), 658–660. https://doi.org/10.1126/science.1092787.
(117) Batista, E. R.; Xantheas, S. S.; Jónsson, H. Multipole Moments of Water Molecules in Clusters and Ice Ih from First Principles Calculations. *J. Chem. Phys.* **1999**, *111* (13), 6011–6015. https://doi.org/10.1063/1.479897.
(118) Baer, M. D.; Mundy, C. J.; McGrath, M. J.; Kuo, I.-F. W.; Siepmann, J. I.; Tobias, D. J. Re-Examining the Properties of the Aqueous Vapor–Liquid Interface Using Dispersion Corrected Density Functional Theory. *J. Chem. Phys.* **2011**, *135* (12), 124712. https://doi.org/10.1063/1.3633239.
(119) Dang, L. X.; Chang, T.-M. Molecular Dynamics Study of Water Clusters, Liquid, and Liquid–Vapor Interface of Water with Many-Body Potentials. *J. Chem. Phys.* **1997**, *106* (19), 8149–8159. https://doi.org/10.1063/1.473820.
(120) Coutinho, K.; Guedes, R. C.; Costa Cabral, B. J.; Canuto, S. Electronic Polarization of Liquid Water: Converged Monte Carlo-Quantum Mechanics Results for the Multipole Moments. *Chem. Phys. Lett.* **2003**, *369* (3–4), 345–353. https://doi.org/10.1016/S0009-2614(02)02026-2.
(121) Raabe, G.; Sadus, R. J. Molecular Dynamics Simulation of the Dielectric Constant of Water:

The Effect of Bond Flexibility. *J. Chem. Phys.* **2011**, *134* (23), 234501. https://doi.org/10.1063/1.3600337.
(122) Izadi, S.; Anandakrishnan, R.; Onufriev, A. V. Building Water Models: A Different Approach. *J. Phys. Chem. Lett.* **2014**, *5* (21), 3863–3871. https://doi.org/10.1021/jz501780a.
(123) Neumann, M. Dipole Moment Fluctuation Formulas in Computer Simulations of Polar Systems. *Mol. Phys.* **1983**, *50* (4), 841–858. https://doi.org/10.1080/00268978300102721.
(124) Shiratani, E.; Sasai, M. Growth and Collapse of Structural Patterns in the Hydrogen Bond Network in Liquid Water. *J. Chem. Phys.* **1996**, *104* (19), 7671–7680. https://doi.org/10.1063/1.471475.
(125) Chau, P.-L.; Hardwick, A. J. A New Order Parameter for Tetrahedral Configurations. *Mol. Phys.* **1998**, *93* (3), 511–518. https://doi.org/10.1080/002689798169195.
(126) Errington, J. R.; Debenedetti, P. G. Relationship between Structural Order and the Anomalies of Liquid Water. *Nature* **2001**, *409* (6818), 318–321. https://doi.org/10.1038/35053024.
(127) Kuyper, L. F.; Hunter, R. N.; Ashton, D. Free Energy Calculations on the Relative Solvation Free Energies of Benzene, Anisole, and 1,2,3-Trimethoxybenzene: Theoretical and Experimental Analysis of Aromatic Methoxy Solvation. *J. Phys. Chem.* **1991**, *95* (17), 6661–6666. https://doi.org/10.1021/j100170a052.
(128) Shivakumar, D.; Williams, J.; Wu, Y.; Damm, W.; Shelley, J.; Sherman, W. Prediction of Absolute Solvation Free Energies Using Molecular Dynamics Free Energy Perturbation and the OPLS Force Field. *J. Chem. Theory Comput.* **2010**, *6* (5), 1509–1519. https://doi.org/10.1021/ct900587b.
(129) Arnold, D.; Plank, C.; Erickson, E.; Pike, F. Solubility of Benzene in Water. *Ind. Eng. Chem. Chem. Eng. Data Ser.* **1958**, *3* (2), 253–256. https://doi.org/10.1021/i460004a016.
(130) Neely, B. J.; Wagner, J.; Robinson, R. L.; Gasem, K. A. M. Mutual Solubility Measurements of Hydrocarbon–Water Systems Containing Benzene, Toluene, and 3-Methylpentane. *J. Chem. Eng. Data* **2008**, *53* (1), 165–174. https://doi.org/10.1021/je700449z.
(131) Perez-Tejeda, P.; Yanes, C.; Maestre, A. Solubility of Naphthalene in Water + Alcohol Solutions at Various Temperatures. *J. Chem. Eng. Data* **1990**, *35* (3), 244–246. https://doi.org/10.1021/je00061a007.
(132) Karásek, P.; Planeta, J.; Roth, M. Solubility of Solid Polycyclic Aromatic Hydrocarbons in Pressurized Hot Water: Correlation with Pure Component Properties. *Ind. Eng. Chem. Res.* **2006**, *45* (12), 4454–4460. https://doi.org/10.1021/ie0514509.
(133) Bradley, R.S.; Dew, M.J.; Munro, D.C. The Solubility of Benzene and Toluene in Water and Aqueous Salt Solutions under Pressure. *High Temperatures-High Pressures*. 1973, pp 169–176.
(134) Sawamura, S.; Tsuchiya, M.; Ishigami, T.; Taniguchi, Y.; Suzuki, K. Effect of Pressure on the Solubility of Naphthalene in Water at 25°C. *J. Solut. Chem.* **1993**, *22* (8), 727–732. https://doi.org/10.1007/BF00647412.
(135) Sawamura, S. Pressure Dependence of the Solubilities of Anthracene and Phenanthrene in Water at 25°C. *J. Solut. Chem.* **2000**, *29* (4), 369–375. https://doi.org/10.1023/A:1005158602563.
(136) Berendsen, H. J. C.; Postma, J. P. M.; van Gunsteren, W. F.; Hermans, J. Interaction Models for Water in Relation to Protein Hydration. In *Intermolecular Forces*; Pullman, B., Ed.; Springer Netherlands: Dordrecht, 1981; Vol. 14, pp 331–342. https://doi.org/10.1007/978-94-015-7658-1_21.
(137) Galamba, N. On the Effects of Temperature, Pressure, and Dissolved Salts on the Hydrogen-Bond Network of Water. *J. Phys. Chem. B* **2013**, *117* (2), 589–601. https://doi.org/10.1021/jp309312q.
(138) Shinoda, K. "Iceberg" Formation and Solubility. *J. Phys. Chem.* **1977**, *81* (13), 1300–1302. https://doi.org/10.1021/j100528a016.
(139) Mateus, M. P. S.; Galamba, N.; Cabral, B. J. C. Structure and Electronic Properties of a

Benzene-Water Solution. *J. Chem. Phys.* **2012**, *136* (1), 014507. https://doi.org/10.1063/1.3671947.
(140) Galamba, N. Water Tetrahedrons, Hydrogen-Bond Dynamics, and the Orientational Mobility of Water around Hydrophobic Solutes. *J. Phys. Chem. B* **2014**, *118* (15), 4169–4176. https://doi.org/10.1021/jp500067a.
(141) Soper, A. K.; Ricci, M. A. Structures of High-Density and Low-Density Water. *Phys. Rev. Lett.* **2000**, *84* (13), 2881–2884. https://doi.org/10.1103/PhysRevLett.84.2881.
(142) Pettersson, L. G. M.; Nilsson, A. The Structure of Water; from Ambient to Deeply Supercooled. *J. Non-Cryst. Solids* **2015**, *407*, 399–417. https://doi.org/10.1016/j.jnoncrysol.2014.08.026.
(143) Galamba, N. On the Hydrogen-Bond Network and the Non-Arrhenius Transport Properties of Water. *J. Phys. Condens. Matter* **2017**, *29* (1), 015101. https://doi.org/10.1088/0953-8984/29/1/015101.

Graphical Abstract

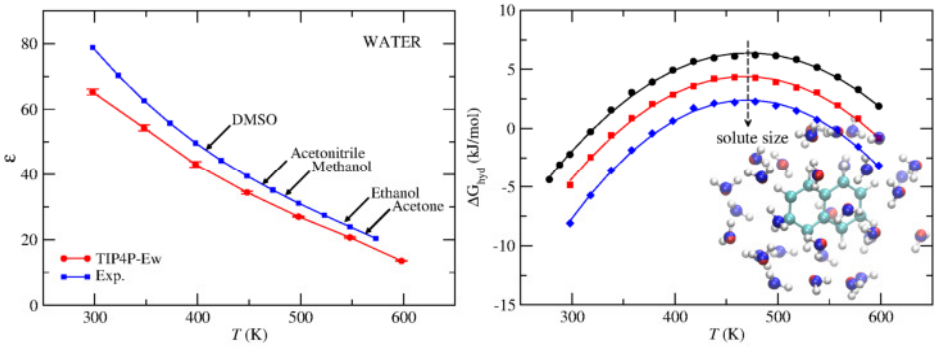

Solubility of Polar and Non-Polar Aromatic Molecules in Subcritical Water: The Role of the Dielectric Constant

Supporting Information

Nuno Galamba[a,*], Alexandre Paiva[b], Susana Barreiros[b], Pedro Simões[b]

[a] *Centre of Chemistry and Biochemistry and Biosystems and Integrative Sciences Institute, Faculty of Sciences of the University of Lisbon, C8, Campo Grande, 1749-016 Lisbon, Portugal.*

[b] *LAQV-REQUIMTE, Departamento de Química, Faculdade de Ciências e Tecnologia, Universidade Nova de Lisboa, 2829-516 Caparica, Portugal*

[*] Corresponding author. Electronic mail: njgalamba@fc.ul.pt

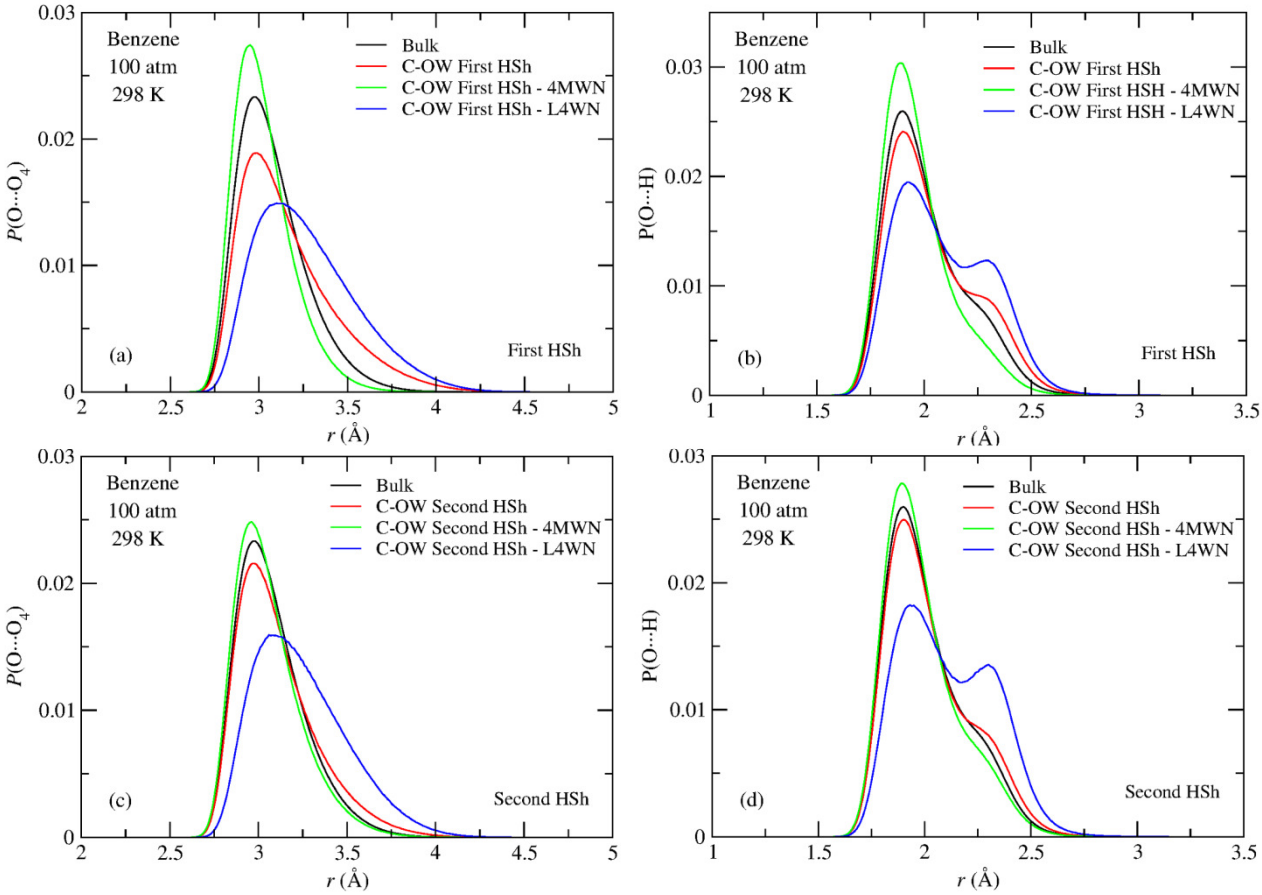

Figure 1-SI - $P(O\cdots O_4)$ and $P(O\cdots H)$ distributions in a benzene aqueous solution at 298 K and 100 atm. (a) and (c): $P(O\cdots O_4)$ distribution of the distance of an O atom to the fourth nearest O atom, for bulk water and for water in the first (F-HSh) and second (S-HSh) hydration shells of the C atoms of benzene; (b) and (d): $P(O\cdots H)$ distribution of the distance of each O atom to the nearest two H atoms of neighbor water molecules for bulk water and for water in the F-HSh and S-HSh of the C atoms of benzene. The boundaries of the C-OW F-HSh and S-HSh are, respectively, $r < 4.2$ Å and $4.2\text{Å} < r < 5.4$ Å; see Fig. 4-SI(b).

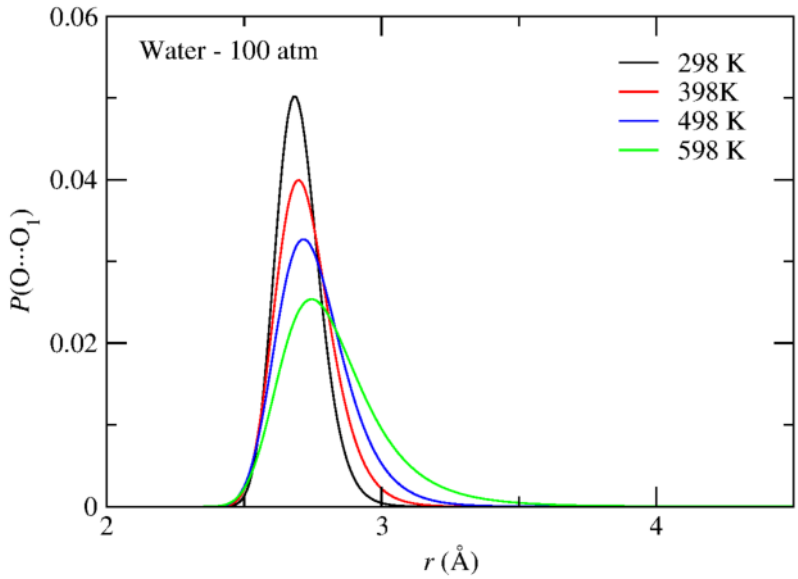

Figure 2-SI - $P(O\cdots O_1)$ distributions in bulk water at 100 atm and temperatures between 298 K and 598 K. The average distance increases from 2.7 Å to 2.8 Å, from 298 K to 598 K; $\Delta V_{void} = V_{void}^{598K} - V_{void}^{298K}$ is ~10

Å^3.

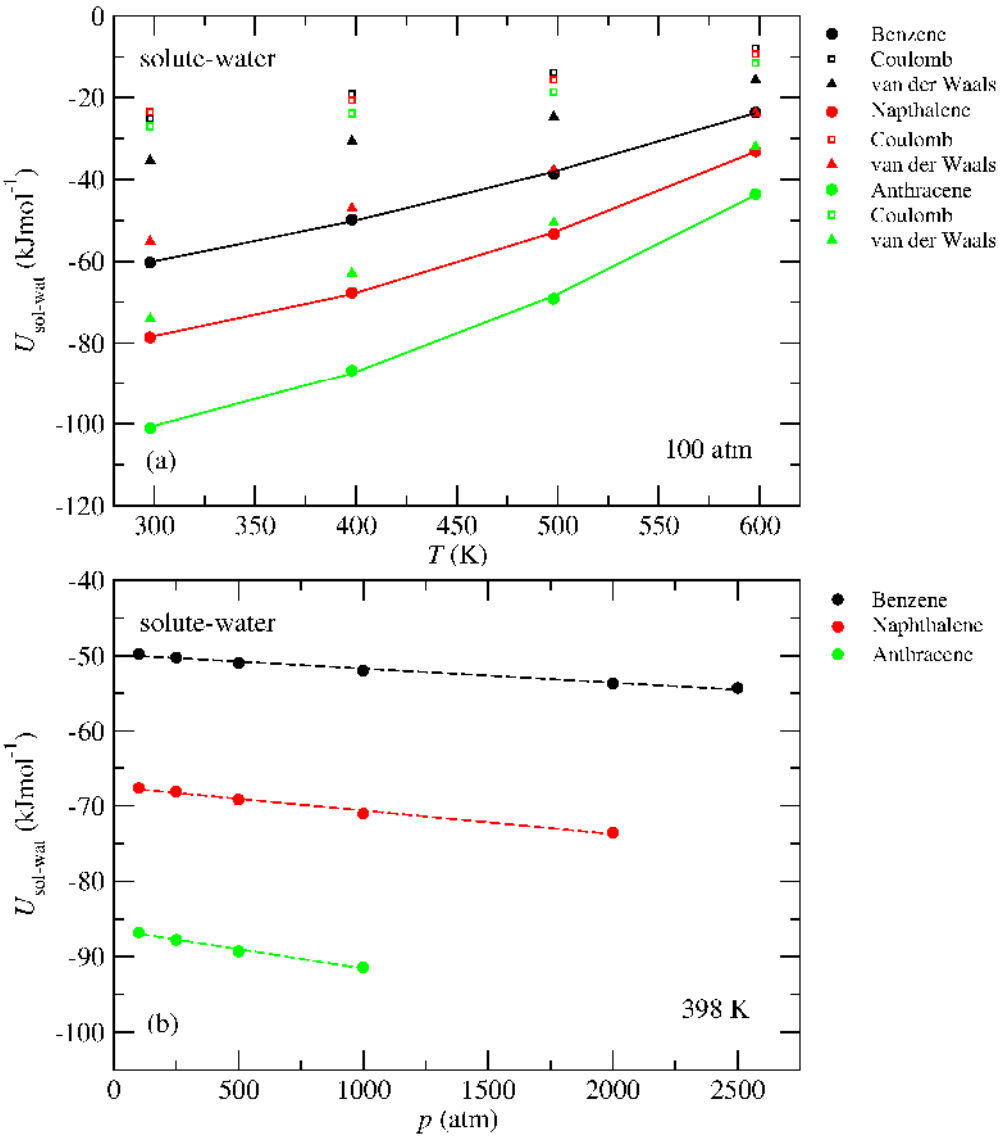

Figure 3-SI – (a) Temperature and (b) pressure dependence of the solute-water non-bonded potential energy for benzene, naphthalene, and anthracene aqueous solutions at 100 atm and 398 K, respectively. The short-range (10 Å) van der Waals and Coulombic components of the potential energy are shown as a function of temperature.

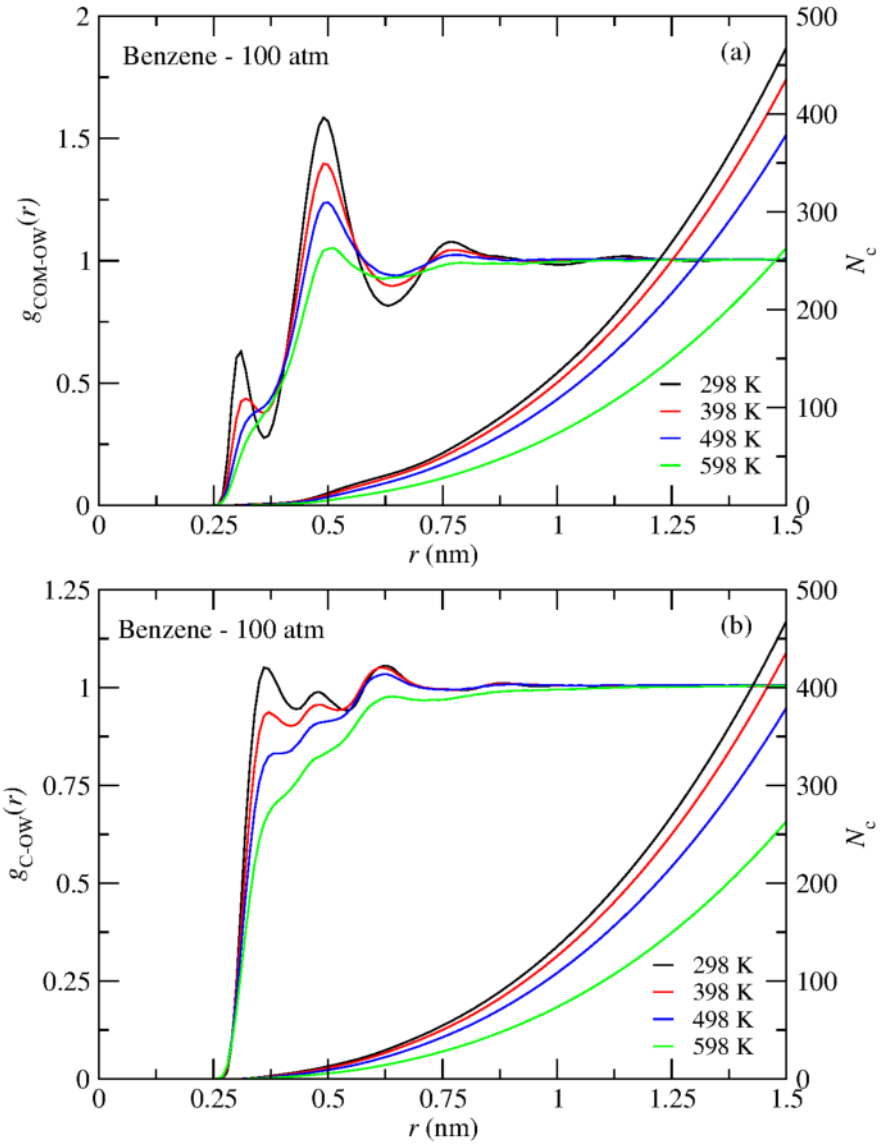

Figure 4-SI – Benzene-water oxygen radial distribution functions, $g(r)$, and coordination number (N_c) at 100 atm and temperatures between 298 K and 598 K. (a) benzene centre of mass – oxygen (COM-OW) rdf and (b) benzene carbon-oxygen (C-OW) rdf. The first peak of the COM-OW rdf, more visible at 298 K, corresponds to ~1.5 hydrogen bonds formed between water and the aromatic ring. The radial distributions functions at 298 K and 1 atm are almost identical and are not shown.

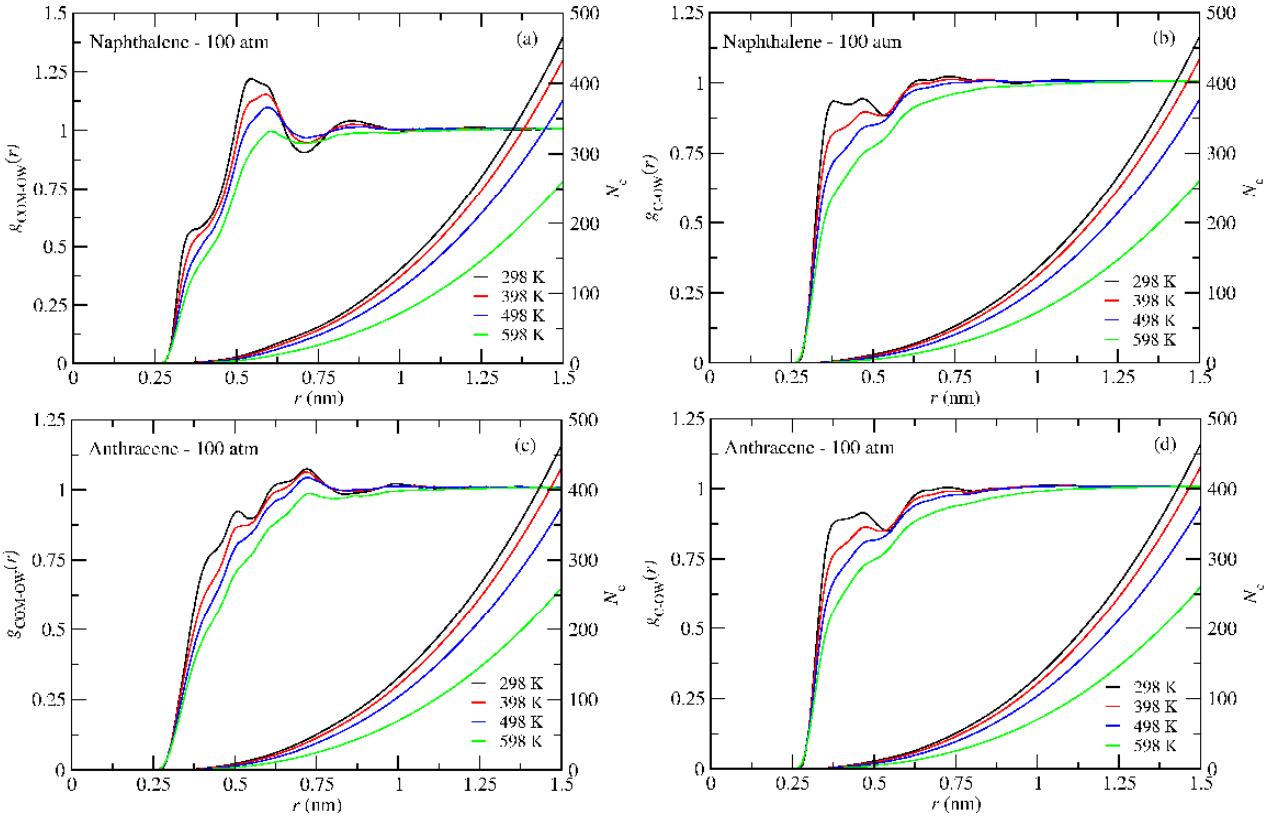

Fig. 5-SI – Naphthalene and anthracene COM-OW and C-OW rdfs and the respective coordination numbers at 298 K, 398 K, 498 K, and 598 K and 100 atm.

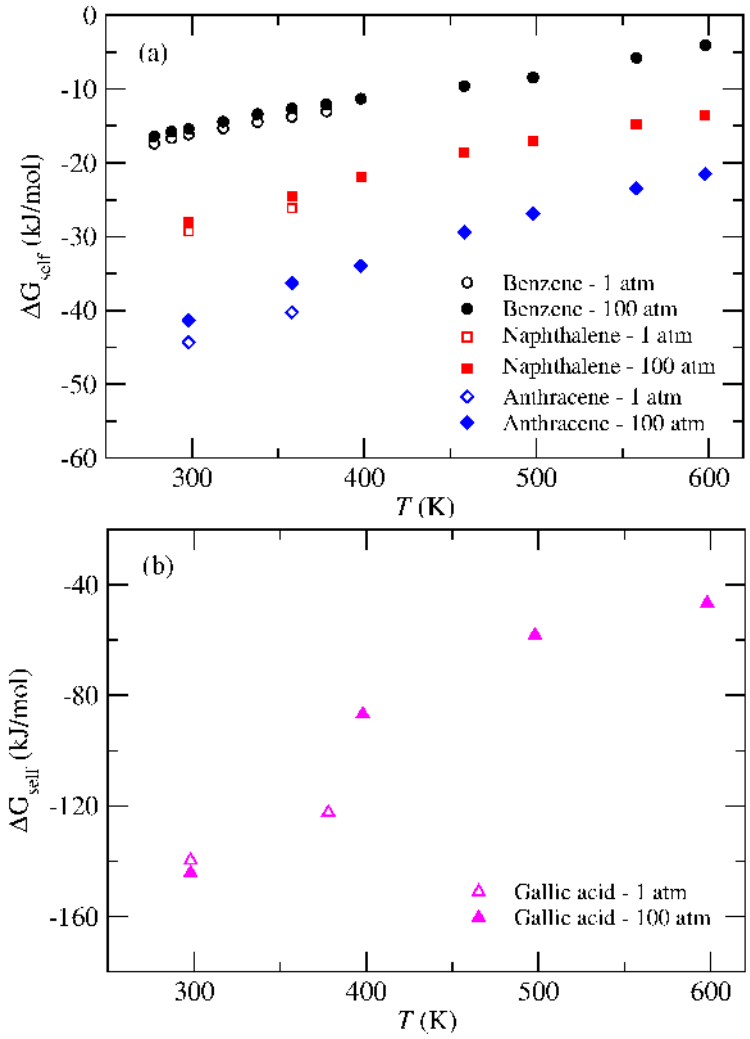

Figure 6-SI – Temperature dependence of the self-free energies for pure (a) benzene, naphthalene, and anthracene, and (b) gallic acid, at 1 atm and 100 atm.

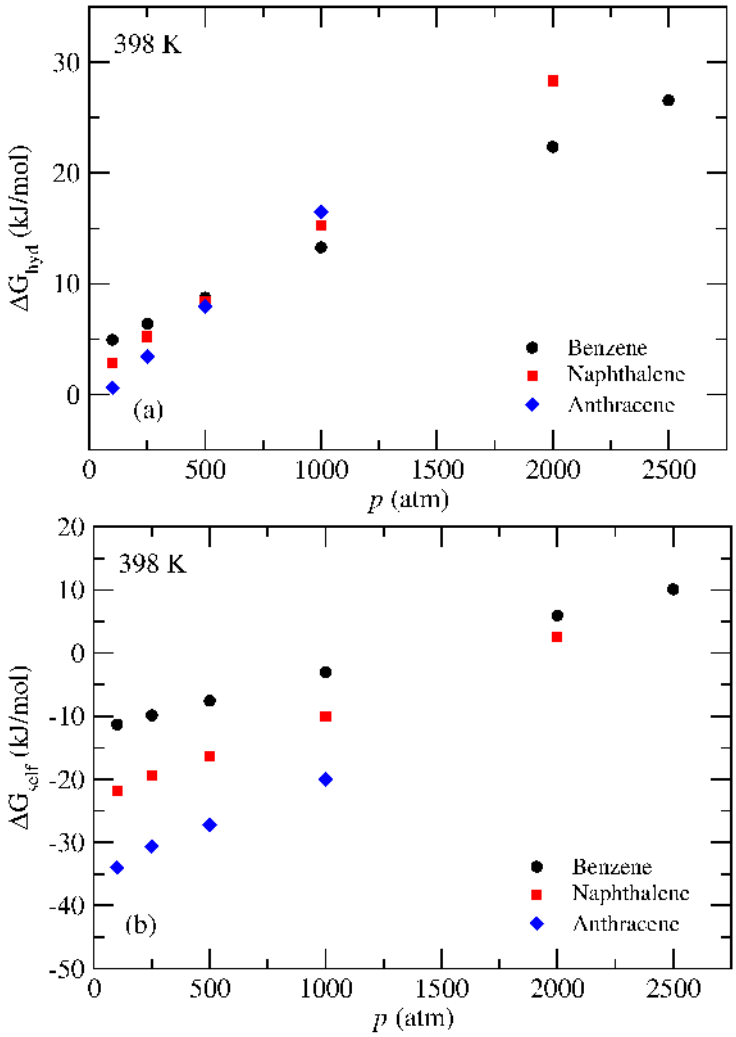

Figure 7-SI – Pressure dependence of the (a) hydration and (b) self-free energies of benzene naphthalene, and anthracene at 398 K.

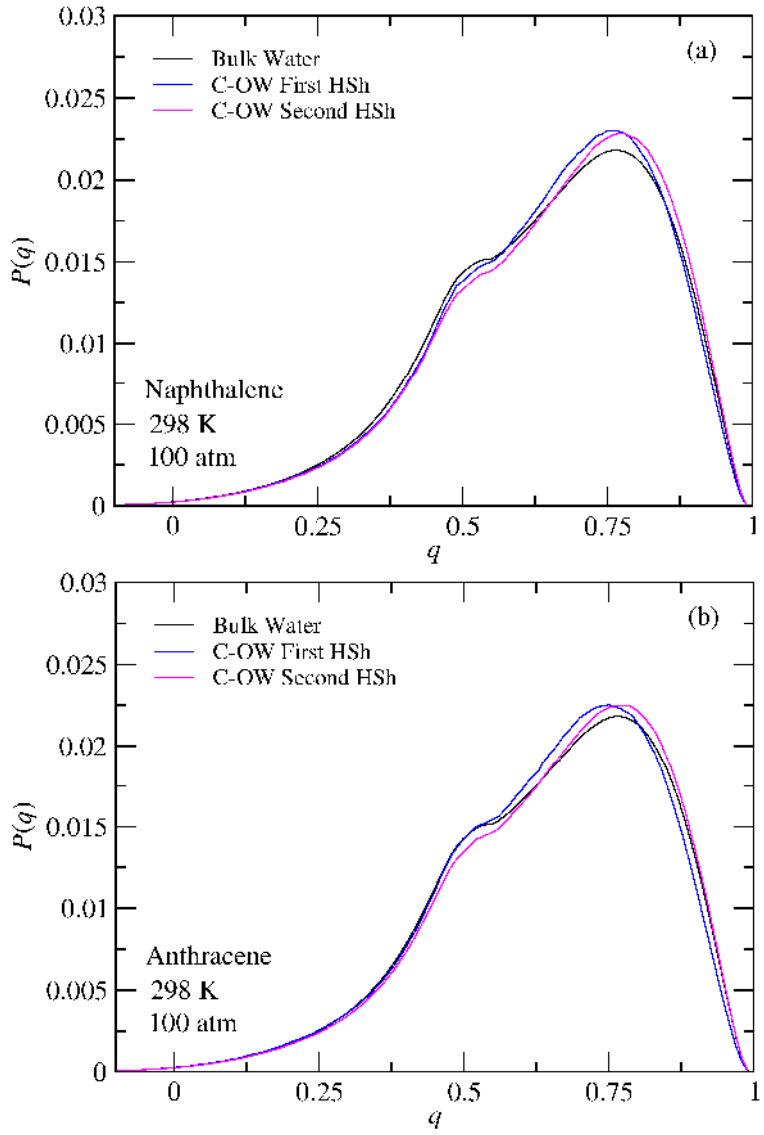

Figure 8-SI – (a) Tetrahedrality, q, of bulk water and water molecules with 4 or more water neighbors (4MWN) in the first and second hydration shells (HSh) of the C atoms of naphthalene and anthracene at 298 K and 100 atm. Water molecules in the HSh of more than one C atom are only counted once in the calculation of q. The 4MWN population represents 46% of the first HSh (N_w = 21.9 and N_w = 26.7, respectively) and 67% of the second Hsh (N_w = 39.7 and N_w = 47.1, respectively) for both solutes. N_w is the number of distinct water molecules in the first and second HSh of the C atoms of naphthalene and anthracene and should not be confused with the coordination numbers, N_c.

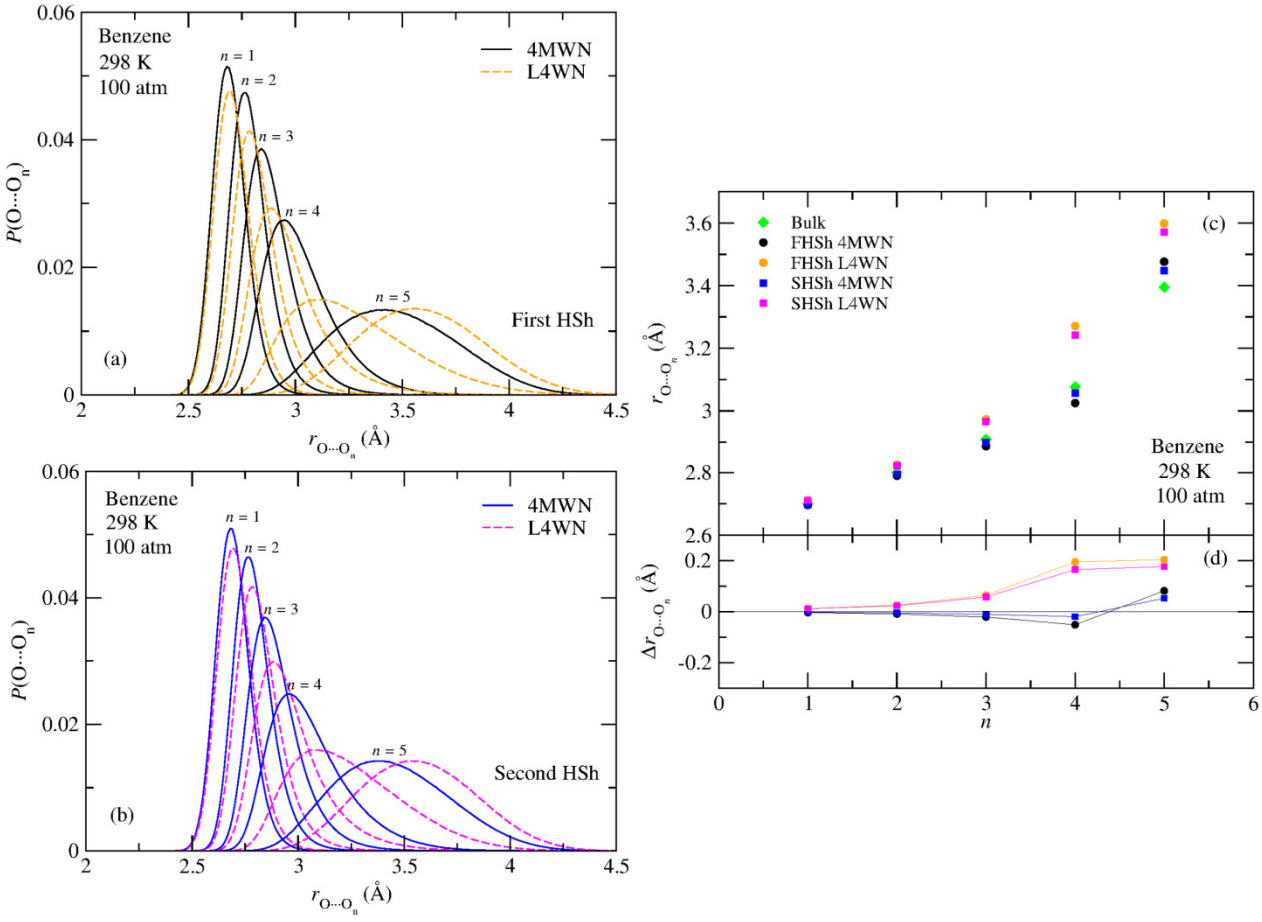

Figure 9-SI - P(O···O_n) distributions for a benzene aqueous solution at 298 K and 100 atm. (a) P(O···O_n) (n = 1 to 5) for water molecules with 4 or more water neighbors (4MWN) and less than 4 water neighbors (L4WN) in the first (C-OW) HSh, (b) P(O···O_n) (n= 1 to 5) for water molecules with 4MWN and L4WN in the second (C-OW) HSh, (c) average $r_{O\cdots O_n}$ for the bulk, first, and second HSh, (d) difference between $r_{O\cdots O_n}$ in the shells and bulk.

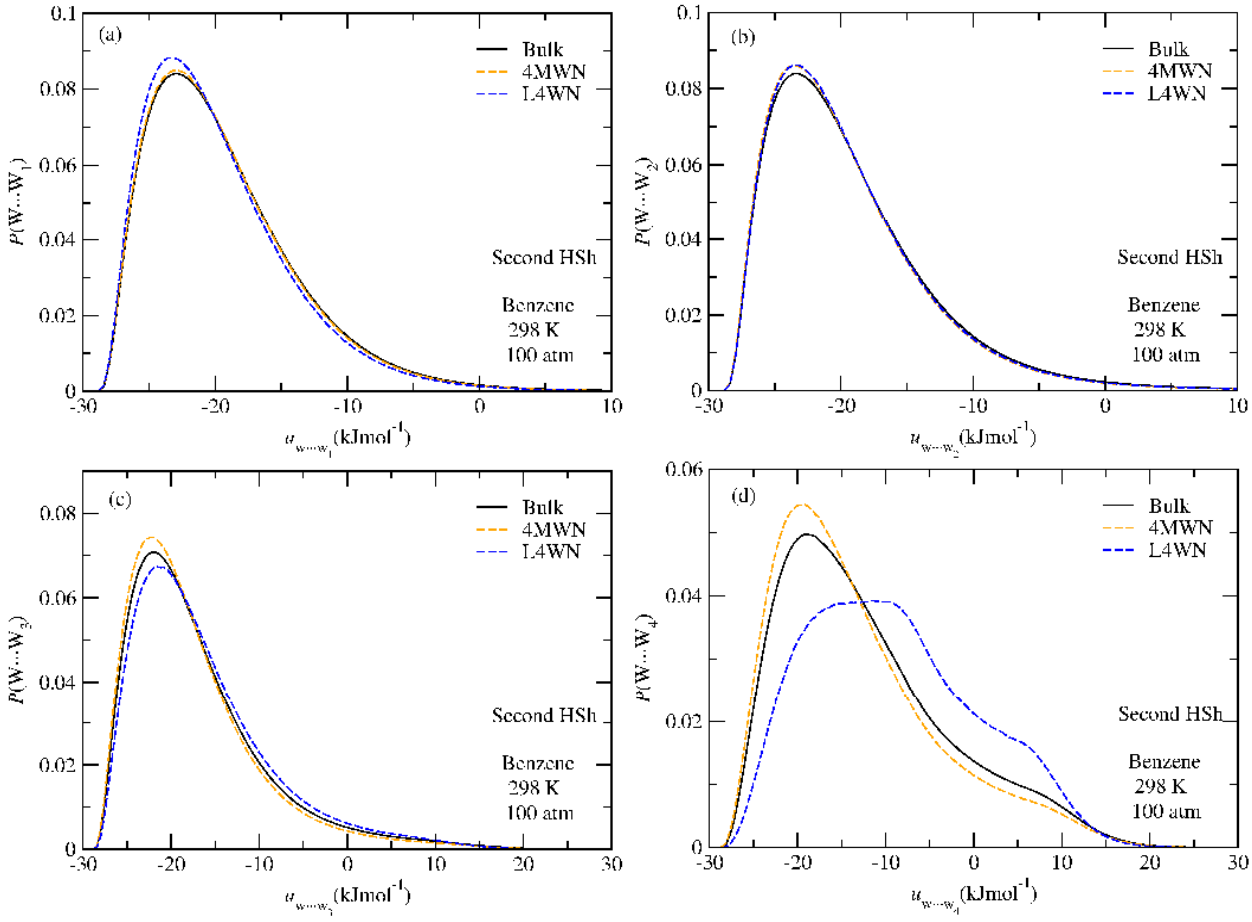

Figure 10-SI - Water pair interaction energy distributions, $P(W\cdots W_n)$ for n = 1 to 4, for bulk water and water with 4MWN and L4WN in the second hydration shell of benzene at 298 K and 100 atm. The N_W with 4MWN and with L4WN is 22.2 and 8.5, respectively. Similar results were found for an aqueous solution at 1 atm; see Table 2-SI to 5-SI. The distributions for the 4MWN and L4WN in (b) are nearly indistinguishable.

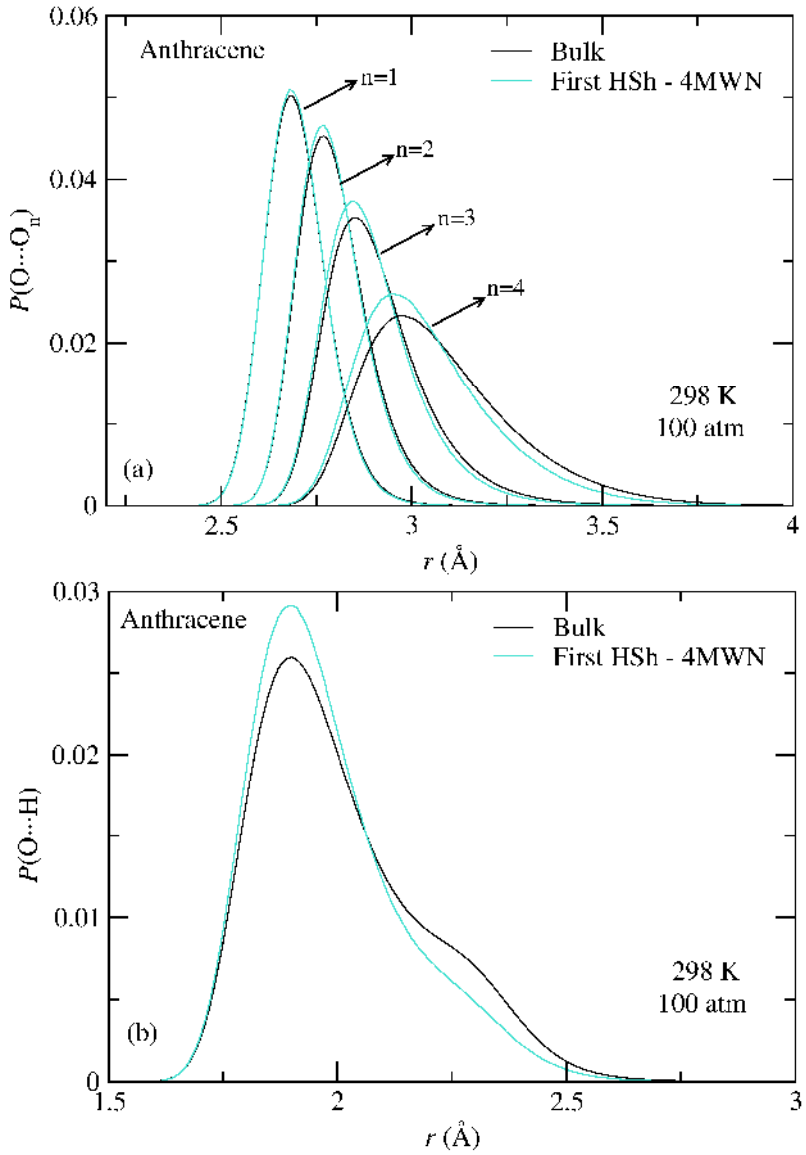

Figure 11-SI – (a) P(O···O_n) and (b) P(O···H) distributions for an anthracene aqueous solution at 298 K and 100 atm. (a) P(O···O_n) (n = 1 to 4) and (b) P(O···H), for the bulk and water molecules with 4 or more water neighbors (4MWN) in the first (C-OW) HSh.

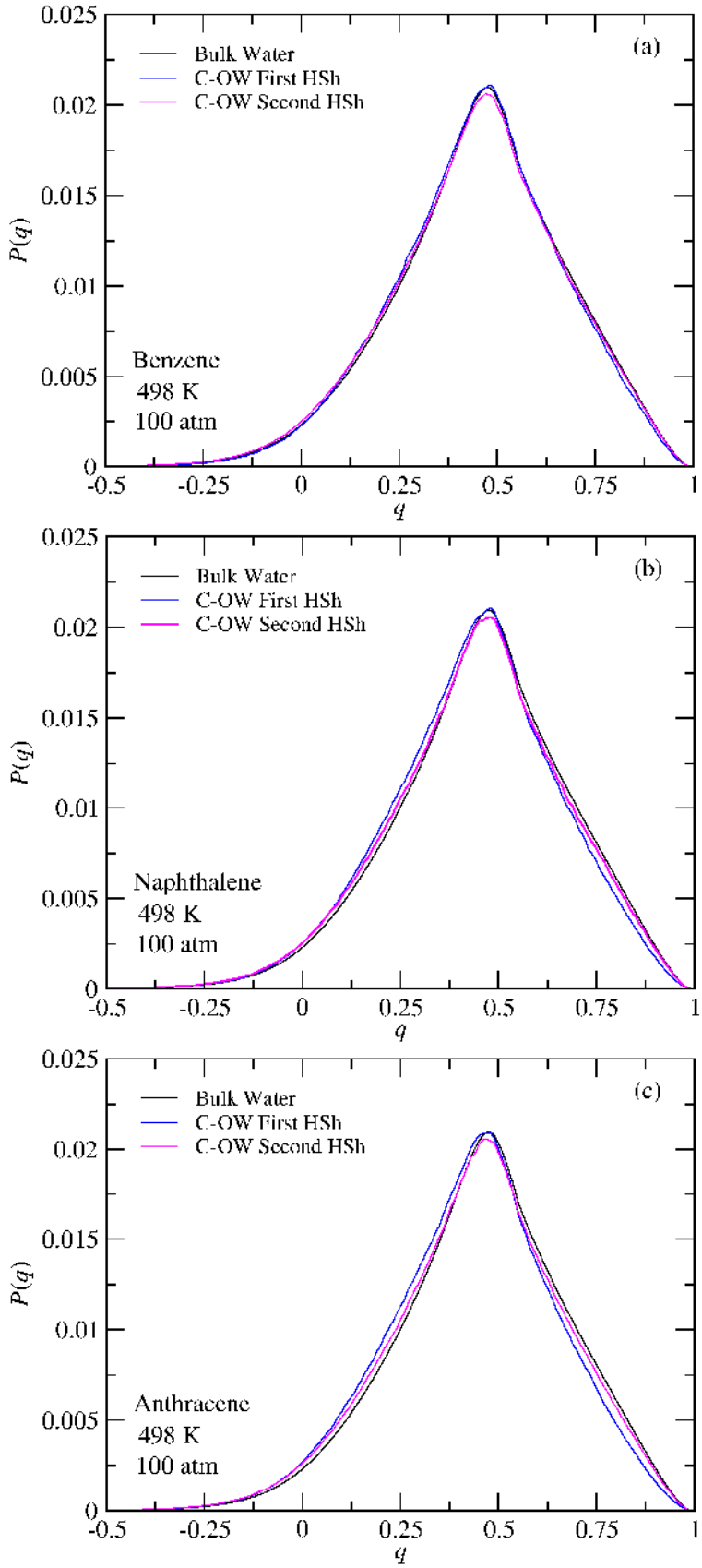

Figure 12-SI – (a) Tetrahedrality, q, of bulk water and water molecules with 4 or more water neighbors (4MWN) in the first and second hydration shells of the C atoms of (a) benzene, (b) naphthalene, and (c) anthracene, at 498 K and 100 atm.

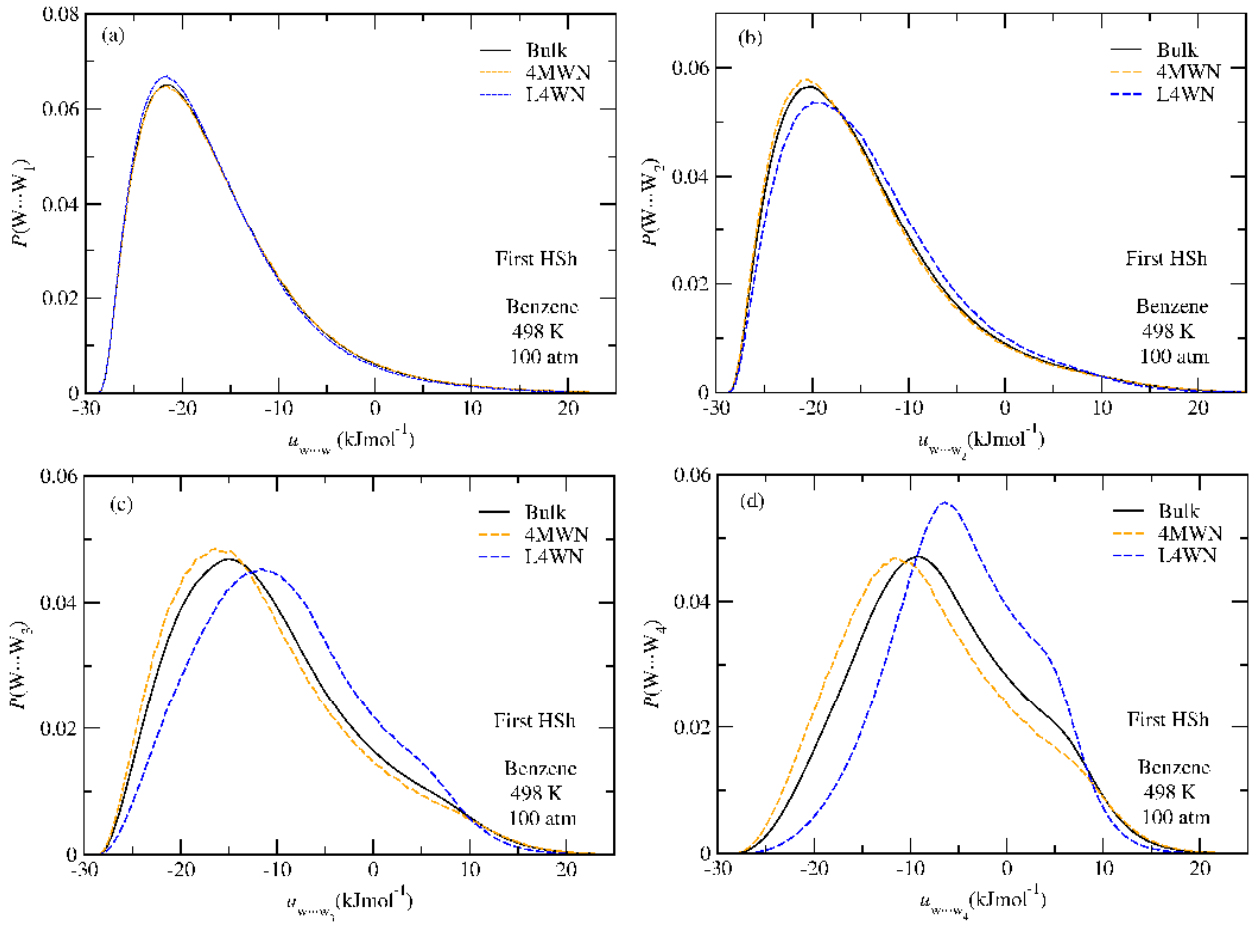

Figure 13-SI – Water pair interaction energy distributions, $P(W\cdots W_n)$ for n = 1 to 4, for bulk water and water molecules with 4MWN and L4WN in the first hydration shell of benzene at 298 K and 100 atm. The N_W with 4MWN and with L4WN are 2.6 and 8.4, respectively.

Table 1-SI – Hydration enthalpy of aqueous solutions of benzene at 298 K and 378 K and at 1 atm and 100 atm, calculated from the hydration free energy and entropy $\Delta H=\Delta G+T\Delta S$ (Fig. 2) and via eq.(9).

T (K)	p (atm)	$\Delta H=\Delta G+T\Delta S$ (kJmol^{-1})	ΔH eq.(9) (kJmol^{-1})
298	1	-34.7	-26.(7)±4[1]
298	100	-31.4	-25.(0)±4
378	1	-13.6	-3.(2)±4
378	100	-16.1	-5.(3)±3

[1] Standard deviations calculated through propagation of the $H_{solution}$, H_{water}, and $U_{sol,vacuum}$ standard deviations calculated from 10 independent trajectories for the aqueous solutions, pure water, and the solute in vacuum.

Table 2-SI – Water-water nth (n = 1 to 5) average pair interaction energies in the bulk and hydration shells (HSh) of a benzene aqueous solution at 298 K and 1 atm. First HSh (FHSh); Second HSh (SHSh).

	n=1	n=2	n=3	n=4	n=5
Bulk	-19.36	-19.25	-17.06	-12.23	-3.19
FHSh - 4MWN	-19.47	19.57	-17.89	-14.16	-2.65
FHSh - L4WN	-19.82	-19.43	-16.27	-8.47	-2.11
SHSh - 4MWN	-19.48	-19.53	-17.65	-13.31	-2.87
SHSh - L4WN	-19.81	-19.45	-16.39	-9.00	-2.17

Table 3-SI – Water-water nth (n = 1 to 5) average pair interaction energies in the bulk and hydration shells (HSh) of a benzene aqueous solution at 298 K and 100 atm. First HSh (FHSh); Second HSh (SHSh).

	n=1	n=2	n=3	n=4	n=5
Bulk	-19.34	-19.23	-17.04	-12.21	-3.21
FHSh - 4MWN	-19.43	-19.55	-17.86	-14.11	-2.68
FHSh - L4WN	-19.80	-19.41	-16.26	-8.49	-2.12
SHSh - 4MWN	-19.47	-19.52	-17.63	-13.28	-2.90
SHSh - L4WN	-19.79	-19.44	-16.41	-9.09	-2.21

Table 4-SI – Water-water nth (n = 1 to 5) average pair interaction energies in the bulk and hydration shells (HSh) of a benzene aqueous solution at 378 K and 1 atm. First HSh (FHSh); Second HSh (SHSh).

	n=1	n=2	n=3	n=4	n=5
Bulk	-18.14	-17.28	-14.13	-9.26	-3.77
FHSh - 4MWN	-18.20	-17.58	-14.90	-10.74	-3.42
FHSh - L4WN	-18.62	-17.26	-12.92	-6.37	-2.58
SHSh - 4MWN	-18.29	-17.58	-14.63	-9.92	-3.58
SHSh - L4WN	-18.63	-17.32	-13.04	-6.50	-2.64

Table 5-SI – Water-water nth (n = 1 to 5) average pair interaction energies in the bulk and hydration shells (HSh) of a benzene aqueous solution at 378 K and 100 atm. First HSh (FHSh); Second HSh (SHSh).

	n=1	n=2	n=3	n=4	n=5
Bulk	-18.11	-17.26	-14.14	-9.28	-3.79
FHSh - 4MWN	-18.18	-17.56	-14.89	-10.75	-3.43
FHSh - L4WN	-18.59	-17.24	-12.94	-6.41	-2.59
SHSh - 4MWN	-18.26	-17.56	-14.63	-9.94	-3.59
SHSh - L4WN	-18.60	-17.31	-13.06	-6.55	-2.65